Summer 5-6-2017

Investigating the classical and non-classical mechanical properties of GaN nanowires

Mohammad Reza Zamani Kouhpanji
University of New Mexico

Recommended Citation

Student Name: Mohammad Reza Zamani Kouhpanji

Candidate

Graduate Unit (Department): Electrical and Computer Engineering

Department

This thesis is approved, and it is accepted in quality and form for publication:

Approved by the Thesis Committee:

Dr. Tito Busani   ,

Chairperson

Dr. Yu-Lin Shen

Dr. Francesca Cavallo

_____

(Note: Type each committee member's name on a single line; this will become the first page of front matter)

_____

_____

_____

_____

Investigating the classical and non-classical mechanical properties of GaN nanowires

By

Mohammad Reza Zamani Kouhpanji

Bachelor of Science, Mechanical Engineering
Master of Science, Mechanical Engineering

Thesis

Submitted in Partial Fulfillment of the Requirements for the Degree of

Master of Science, Electrical Engineering

The University of New Mexico

Albuquerque, New Mexico

July 2017

Investigating the classical and non-classical mechanical properties of GaN nanowires

By
Mohammad Reza Zamani Kouhpanji
M.S., Electrical Engineering, University of New Mexico, 2017

Abstract

Study and prediction of classical/non-classical mechanical properties of GaN is crucial due to the potential application of GaN nanowires (NWs) in piezoelectric, probe-based nanometrology, and nanolithography areas. GaN is mainly grown on sapphire substrates whose lattice constant and thermal expansion coefficient are significantly different from GaN. These discrepancies cause mechanical defects and high residual stresses and strains in GaN, which reduce its quantum efficiency.

Specifically, for nanoscale applications, the mechanical properties of materials differ significantly compared to the bulk properties due to size-effects. Therefore, it is essential to investigate the mechanical properties of GaN NWs using the non-classical solid mechanic theories, modified couple stress theory (MCST) and modified strain gradient theory (MSGT).

Experimentally the GaN NWs were prepared by using top-down approach to etch c-plane GaN layer grown in Metal Organic Chemical Vapor Deposition (MOCVD) chamber to achieve high aspect ratio NWs with high uniformity. An Atomic Force Microscope (AFM) was used to apply an infinitesimal deflection on the top of clamped-free NWs while monitoring the lateral and normal forces.

According to the MCST, the Young's modulus, shear modulus and length scale were measured to be 323 GPa, 133 GPa and 13 nm, respectively, and according to the MSGT, they were measured to be 319 GPa, 132 GPa and 8 nm, respectively. Furthermore, a quantum mechanics based approached was conducted to estimate the classical/non-classical mechanical properties of the GaN NWs as well.

TABLE OF CONTENTS

LIST OF FIGURES

LIST OF TABLES

Chapter 1: literature Review

1- **Introduction**

In This chapter, a brief review about the GaN NWs applications, the importance of determining the mechanical properties of GaN NWs and the size-effects of mechanical properties of GaN NWs are presented. The next sections consist of the available experimental techniques for measuring the mechanical properties of NWs and the progress in non-classical theories in solid mechanics have been provided as well.

2- **GaN NWs**

GaN as a wide bandgap semiconductor has attracted many attentions in electronics and photonics areas because of its chemical stability in high temperatures and high frequencies. It also presents high mobility of electrons at the interfaces of semiconductor heterostructures which makes it appropriate for blue-green and UV light emitting diodes, laser diodes, active and passive parts in nanosensors and high- power/temperature transistors [1-6]. It is noteworthy to be mentioned that the application of the GaN is not restricted only to electronic and photonic devices. It has been shown that they are an exceptional candidate for other applications, such as probe-based nanometrology, nanolithography and piezoelectric applications [7-8].

Extensive progress on GaN in recent years made it possible to fabricate various geometries such as NWs [9-10], nanotubes (NTs) [11] and single walls nanostructures (SWN) [12] applicable for many applications such as actuators and sensors. Regarding to the superior quantum confinement effects of GaN NWs [13], fabrication and

characterization of optical properties, electrical properties and mechanical properties, of GaN-based NWs devices became one of the most important and active research areas in different engineering fields and science. So far, investigations and developments of GaN-based NWs devices have mainly focused on the synthesis, physical properties and chemical properties of these devices [14]. Comparing to the numerous studies of optical and electrical properties of GaN-based NWs devices, their mechanical properties have been less investigated because of the difficulty of mechanical testing of nanodevices. However, the mechanical properties of, not only GaN-based NWs devices, but also all semiconductor-based devices, have a crucial factor in performance of these devices in different operation conditions. That is why GaN NWs are mainly grown on sapphire substrates whose lattice constant and thermal expansion coefficient are significantly different from GaN. These incompatibilities cause mechanical defects and high residual strains/stresses in GaN NWs. The mechanical defects drastically decrease the device performance by reducing the mobility of the carriers and inducing inhomogeneous distributions of the carriers in the active region [15-16].

It has been theoretically and experimentally shown that material dimensions have significant effects on the mechanical behaviors of materials, particularly when the dimensions are reduced to the nanometer regimes where many semiconductor-based devices exhibit unusual mechanical properties that significantly different from those of bulk semiconductors. Taking advantages from this size-effects, the physical properties of semiconductor devices can be tuned by applying appropriate mechanical strains/stresses [17]. Consequently, before GaN NWs, or even any semiconductor materials, can be

successfully incorporated into devices, it is important to gain a better understanding of their mechanical behaviors and try to manipulate them to achieve high performance devices.

Extensive theoretical calculation/simulations and experimental measurements have been developed to estimate the mechanical properties and mechanical behaviors of GaN-based NWs devices. Two major approaches of the theoretical calculations/simulations are molecular dynamics simulations and first-principles calculations. These two approaches are powerful tools in investigation of the mechanical behavior of GaN-based NWs devices because they enable the real-time observation of the deformation at the atomic scale, and at the same time, in addition they provide stress-strain curves [18]. Consequently, these theoretical methods have been developed to investigate the mechanical properties of GaN NWs, SWNs and NTs under tension, torsional and bending loads [19-22].

However, the theoretical calculations/simulations require several parameters and imperial functions that they must be accurately determined before being implemented in simulations to predict the mechanical properties of GaN NWs. Moreover, it is noteworthy to be mentioned that the theoretical approaches have unavoidable limitations associated with time-consuming computations. Due to computational limitations, theoretical calculations have been used to study semiconductor-based devices with relatively small diameters, usually below 20 nm. Furthermore, the strain rates applied in simulations are very high, several orders larger than the strain rate of applied strain rate in experiments [18]. Therefore, it is critical to conduct well-design experiments to measure the deformation behaviors of GaN NWs and associate them with the theoretical methods to confirm the computational results.

Since the related experimental methods proved that the preparation methods, nanostructures sizes and measurement techniques suggest different quantities, this is crucial to determine the mechanical properties of GaN NWs based on a well-designed measurement technique to avoid any possible failure of the GaN-based NWs devices. Some of experimental methods have been developed including uniaxial tensile test [23] or uniaxial compressive test [24], *In Situ* TEM/SEM resonance [25-28], three-point bending [29-30] and nanoindentation [31] of GaN NWs. However, due to the small dimensions of GaN NWs and uncertainties of these experiment methods, the mechanical properties of these devices are still challenging and suffering from dispersive values.

Table 1-1 shows the results of the earlier studies in determining the Young's modulus and the Poisson's ratio of GaN NWs. As it can be seen, the reported values are very dispersing. This inconsistency can be explained by scrutinizing the experiments and theoretical analysis used to extract the mechanical properties of GaN NWs. From the experiments aspect, for example, in the uniaxial compression tests, the tensile tests, the three point-bending tests, and nanoindentation tests, the nanostructures are in contact with elastic substrates whose deformations cannot be ignored in some extends [40-42]. The deformations of the substrates change the boundary conditions resulting to overestimate the true value of the nanostructures deformations. Furthermore, in these experiments, regardless of the difficulties of preparing the samples, the GaN NWs need being transferred and welded on a MEMS-/NEMS-based device or a trench, that can change the mechanical properties of GaN NWs due to contaminations and partial fractures of GaN NWs during preparation processes [43].

Table 1-1: experimental and theoretical available mechanical properties of GaN NWs.

	Property	Method	Max.	Min.	Ref.
Experimentally	Young's modulus (Gpa)	Three-point bending	400	194	[30]
		Electromechanical resonator	305	227	[27]
		Nanoindentation	292	298	[31]
		Laser Doppler vibrometry	321	201	[32]
		Uniaxial tensile test	250	210	[23]
		Uniaxial compression test	484	223	[24]
		in situ TEM	319	280	[26]
			404	258	[33]
	Poisson ratio	X-ray diffraction	0.18	0.186	[34]
		Brillouin scattering	0.152	0.252	[35]
		Raman spectroscopy	0.211	0.213	[36]
Theoretically	Young's modulus (Gpa)	First principle	444		[37]
		Electron backscatter diffraction	479		[38]
		Molecular dynamic simulation	290	166	[21]
	Poisson ratio	Linear muffin-tin orbital	0.12		[16]
		First principle	0.212		[39]

From the analysis aspect, in all these studies the Classical Continuum Theory (CCT), also named classical beam theory, was used to extract the mechanical properties of GaN NWs from the experimental data. It is experimentally proved that the CCT is unable either to demonstrate the size-dependency of mechanical behaviors of GaN NWs or to estimate the self-stiffness of GaN NWs [44]. That is why the CCT only considers the displacement components of nanostructures deformation without considering the effects of micro-rotations components, associated with the strain gradients, on the total deformation of the nanostructures [44-45], it will be explained in the following sections with more

details. To take these micro-rotations into account, the non-classical continuum mechanics theories, like modified couple stress theory (MCST) and modified strain gradient theory (MSGT), have been introduced and developed by several researchers [46-48]. In these theories beside the classical materials constants, related to the displacement components, additional material parameters, related to the micro-rotation components, are appearing which enable the theory to demonstrate the size-dependency behaviors of nanostructures.

3- Experimental techniques

Techniques used to estimate the mechanical properties of GaN nanostructures differ from each other based on the desired mechanical properties and the platforms used for the characterization. Due to the small dimensions of nanostructures, all characterization techniques were conducted in one of the following types of microscopes: Atomic Force Microscope (AFM), Scanning Electron Microscope (SEM), and Transmission Electron Microscope (TEM). Here, we categorize and review the existing techniques for characterization of mechanical properties of nanostructures from the literatures based on their loading modes and the required equipment.

3-1- Bending

The most common tools for conducting the bending tests are TEM, SEM and AFM. Any bending test requires the NWs to be prepared either as cantilever, one free end and one fixed end, then applying a lateral force on the free end, or as clamped-clamped NWs, then applying a bending force at any point along the nanostructure. Bending of a cantilever NW is more popular test because of its simplicity; however, it carries a vast amount of

attentions. Nanostructures that epitaxially grown/etched down are perpendicular to the substrate, one end of the NWs has been fixed at the substrate, the experiment can be easily conducted through applying a lateral force perpendicular to the nanostructure axis at the free end of the nanostructure using an AFM/indenter probe [43, 49]. The bending tests can also be conducted in TEM and SEM using special sample holders equipped with AFM indenter systems.

TEM and SEM provide the real-time high-resolution images enabling direct observation of the nanostructure deformation process to understand the deformation mechanisms of nanostructures, in addition to providing the force-displacement curve usable for predicting the mechanical properties of NWs. Noted, the TEM has more advantages over the SEM method because of the higher resolution images; however, TEM needs ultrahigh vacuum that may damage the surface of nanostructures. Furthermore, some bending tests using SEM do not provide any force-displacement curve but the quantitative strength and strain values of nanostructure at fracture can still be calculated.

3-2- In Situ Resonance

The resonance method was first used to characterize the mechanical properties of multi-walled carbon nanotubes and has been applied to other semiconductors nanostructures. In the resonance method, a single cantilever NW is excited by alternating current, AC current. The AC current forces the cantilever NW to resonate at its natural frequency. The method can be used either in TEM or SEM with a specific conductive TEM/SEM specimen holder that delivers the electrical current signals between the tip, to

which the NWs are mounted, and a counter electrode to generate a fluctuating electrical field applying an electrodynamic force to the NW [50].

A sharp tip, usually tungsten tip, is swept against NWs so that some nanostructures from the substrate stick to the tip. The tip is then loaded onto the especial TEM/SEM specimen holder with electrical connection to the tip and a counter electrode and moved precisely to position an individual NW very close to the counter electrode. Applying a tunable AC current across the tungsten tip, where the NW is stuck, and the counter electrode will drive the NW to vibrate mechanically, from which the natural resonant frequency is measured. Noted, the frequency–amplitude relationship determines the resonance frequency. That is why the frequency of the driving voltage is equal to the resonant frequency, at which the NW resonates with the largest amplitude. According to the solid mechanic theories, the resonance frequency of the NW depends on the elastic modulus of the nanostructure. It is worthy to be mentioned that the in situ TEM electric-field-induced resonance method can be easily used to investigate the fatigue behavior of NWs as well [51].

3-3- Uniaxial loading

Characterization of the mechanical properties of NWs can also be accomplished by uniaxial tension or compression loading of a single NW in either TEM or SEM. Tensile tests in SEM requires a NW to be clamped on the tungsten tip of a nanomanipulator at one end and the other end to be fixed on an AFM cantilever using different techniques, such as electron-beam-induced deposition (EBID) or focused ion beam (FIB) implementation. The AFM cantilever works as the load sensor during the measurement while a tensile force is

applied to the NW through the precision movement of the nanomanipulator. The results of this measurement are stress–strain curves, from which the Young's modulus, fracture strength, elastic strain, yield strength and ductility of individual NWs can be predicted. Similar to the uniaxial tensile test, the same experimental setup can be utilized for compression tests of individual NWs in SEM while the nanomanipulator moves precisely toward the AFM cantilever in the opposite direction to apply compressive load to the NWs. However, the uniaxial compression tests are mainly done using a nano-indenter to compress the NWs. The uniaxial compression test cannot be performed for high aspect ratios, length to diameter ratio, NWs because of high chance of buckling. However, this method makes it possible to measure critical buckling load of the NW as well [52-53].

Deforming an NW in SEM using an AFM probe or nanomanipulator enables direct real-time observation of the structural changes during the entire process of the NW deformation. The large chamber size in SEM makes it easy to manipulate the NW deformation processes. However, it is difficult to reveal the deformation mechanisms of NWs during *In Situ* testing in SEM because of the poor structural resolution of SEM. This problem can be overcome by conducting *In Situ* experiments in TEM.

3-4- Nanoindentation

One of the most popular methods for the investigation of mechanical properties of nanomaterials, especially thin films, is nanoindentation. In this method, an indenter, whose tip radius is few nanometers, is pushed into a nanostructure. The results are the applied force vs. the penetration depth which can be easily used to estimate the Young's modulus and hardness, the resistance to permanent or plastic deformation, of the nanostructures. For

nanoindentation of individual NWs, it is necessary to firmly fix the NW to avoid any movements. To do so, an NW is lying flat on the substrate, and both ends of the NW are fixed on the substrate usually by EBID. Nanoindentation can be done either using an AFM tip or an especial indentation tools to perform indentation. The indenter must be much stiffer than the nanostructure, both substrate and thin film or NW, to prevent any possible errors due to local deformation of the indenter. Cares must be taken especially in the case of nanoindentation of NWs with a conical indenter. That is why the indenters are likely to slip and apply friction between the indenter tip and the NW surface during the indentation because the indenter rarely can be perpendicular to the surface of circular-shaped NWs. This issue can be solved by utilizing a Berkovich (three-sided pyramidal diamond) indenter to perform the imaging and indentations [54].

4- Solid mechanic theories

The CCT provided a fundamental basis for analysis and understanding the mechanical behavior of materials on macro scale for two centuries by the initial work of Poisson and Cauchy in 1820s. The CCT uses only displacement components of the nanostructure deformation without considering the independent rotational components of the nanostructures. The displacement components of nanostructure deformation, which also known classical stresses, are related to the external forces using Lame constants, also named classical parameters. While, the independent rotational components of nanostructure deformation, which also known as non-classical stresses or couple stresses, are related to the external forces using length scale, also named non-classical parameter. Simply said, the CCT is not adequate in capturing any size effect or self-stiffness of

10

nanostructures, since it possesses no characteristic length in the governing equations. Therefore, it is necessary to resort to higher order continuum theories, such as MCST or MSGT, which consider the effect of microstructure by including explicit material length scales in their governing equations. Furthermore, these non-classical solid mechanic theories can provide a more suitable connection to atomistic models and the fundamental base for developing size-dependent multi-physics formulations, such as those involving electromechanical coupling.

A review of the early literature reveals that classical continuum mechanics was based initially upon an atomistic representation of materials having only central forces within particles. Equivalently, classical stress and strain components induced by the external forces, describe the internal forces in the continuum model [55]. However, in a more realistic representation of materials, it is essential the introduction of non-central forces, especially when the dimensions are in order of nanometers, in the underlying atomistic models. This was a motivation for many researchers to consider also the effects of the gradients of strains, inducing couple-stresses, in the corresponding continuum representation of the materials.

4-1- Cosserat theory

The Cosserat brothers [45] proposed and formulated different theories for structural elements in one-dimensional space, such as beams, and two-dimensional space, such as shells, embedded in three-dimensional space. In these theories, besides the three independent displacement components, three independent rotational components were considered to fully determine the deformations of materials, six degrees-of-freedom, at

11

each point. Based upon these successes, the Cosserats then extended this idea of independent rotational degrees-of-freedoms to the case of a full three-dimensional elastic medium.

Nowadays, these formulations are referred to as micropolar theories, which attempt to capture the effect of discontinuous microstructure by considering a continuous microrotation in addition to the translational degrees-of-freedom. The concept of independent rotational degrees-of-freedom may also originate from the discrete model of material in molecular point of view. In molecular view, because we are only dealing with one particle, the lumped part of matter can be modeled as rigid bodies, which is the basis of molecular dynamic simulations. In this point of view, the motion of each part can be described by motion of its center of mass and its rotation. In rigid body dynamics, this rotation is independent of the motion of the center of mass [56].

Therefore, describing the translation and rotation of individual particles, such as atoms, molecules and grains, requires discrete point functions. However, in a continuum representation of mechanical behavior of materials, it is assumed that material is continuously distributed in space. As a result, the deformation of the body is represented by the continuous displacement field without considering the discontinuous microstructure of material and motion of individual particles, which has been shown to be inconsistent with experimental works.

4-2- Couple stress theory (MTK model)

Some researchers, such as Mindlin and Tiersten [57], and Koiter [58], believed that the continuous displacement field components are the basis to determine the kinematical

quantities and measures of deformation. Therefore, they speculated that in a consistent continuum theory, the deformation is completely specified by the continuous displacement field. It should be mentioned, in Mindlin-Tiersten-Koiter (MTK) theory, the rigid body motion of the infinitesimal element of material at each point of the continuum is described by six degrees of freedom (i.e., three translational and three rotational). As a result, energy considerations show that higher order measures of deformation must be related to the rotation field.

The main problem in this development is the inconsistency of the boundary condition for the normal component of the moment traction. That is why the right-hand side of the principle virtual work shows that the boundary conditions on the surface of the body can be either displacement vector or rotation vector as essential (geometrical) boundary conditions, or stress and couple stress components as natural boundary conditions [56]. This apparently makes a total number of six boundary values for either case. Consequently, there is no other possible type of boundary condition in size-dependent couple stress continuum mechanics.

However, this contrasts with the number of geometric boundary conditions that can be imposed [58]. This shows that a material in couple stress theory does not support independent distributions of normal surface moment (or twisting) traction, and the number of mechanical boundary conditions also is five. This result was first established by [58] although his couple stress theory does not satisfy this requirement.

4-3- Modified couple stress theory (YCLT model)

After development of MTK theory, some researchers, such as Yang et al. [59], managed to develop a model of couple stress that results in a symmetric couple stress tensor. To do so, they considered an additional equilibrium equation for the moment of couple stresses associated with the two equilibrium equations of the classical continuum. Application of this equilibrium equation leads the curvature tensor to be deviatoric, and thus is specified only by five independent components. Therefore, in this model, which called MCST, all the inconsistencies in MTK theory, such as the indeterminacy in the couple-stress tensor, remain intact.

Interestingly, the stress-strain tensor and the final governing equilibrium equations are similar to those in MTK theory for isotropic material. Regardless of this fact that the MCST inherits all inconsistencies from indeterminate MTK theory, it has been widely attracted attentions in many literatures, because the appearance of only one length scale parameter for isotropic material makes the MCST more desirable from an experimental and analytical view [56]. As a result, this theory has been extensively used in many problems, such as bending, buckling and post-buckling, and vibration in recent years to investigate the mechanical behaviors of the nanostructures [60-61]. It is noteworthy to be mentioned that the MCST cannot be taken as a special case of indeterminate MTK theory. This is obvious by noticing that this similarity is only valid for isotropic material, and there is no simple analogy for general anisotropic and bi-anisotropic cases.

4-4- Modified strain gradient theories

In 1965, Mindlin [62] proposed a higher-order gradient theory for elastic materials by considering the higher derivatives of the strain tensor, from first up to third derivatives, in definition of energy. [62-64] used Mindlin's formulations by considering only the first derivative of the strain tensor and called it the strain gradient theory. In comparison with the couple stress theory, the strain gradient theory contains some additional higher-order stress components beside the classical and couple stresses. Indeed, the couple stress theory is a special case of the strain gradient theory.

In a similar way utilized by Yang et al. [59] for the MCST, Lam et al. [65] introduced a MSGT, which reduces in a special case to the MCST. Henceforth, when the strain gradient theory is used in the text, it denotes the version of the theory presented by Lam et al. [65]. The strain gradient theory is employed to formulate the static and dynamic behaviors of linear and nonlinear elastic beams, both the Euler-Bernoulli and the Timoshenko models, shells and bars under torsional loading. In addition, the size-dependent functionally graded beam models have been developed by Kahrobaiyan, Asghari, Rahaeifard, and Ahmadian [66] based on the strain gradient theory. Furthermore, this non-classical theory is utilized by Akgoz and Civalek [67] to study the buckling of microbeams under uniaxial compression loadings.

Chapter 2: Modified Couple Stress Theory

1- Introduction

In this chapter, a rigorous method for deriving the MCST's governing equations for GaN NWs is provided. The MCST governing equations can be derived based on either energy principle or equilibrium method [46, 48, 59-60]. The procedure presented here is a simplified version of earlier works [48, 59], where they derived the MCST's governing equations based on the energy principal theory. After rederivation of the MCST's governing equations, the governing equations were solved according to the loading and boundary conditions of the GaN NWs to derive the relationship between the deflection and applied force for each individual the GaN NWs.

2- The MCST for elasticity

The modified couple stress theory was presented by Yang et al. [59], in which the both strain tensor (conjugated with classical stresses) and curvature tensor (conjugated with couple stresses or non-classical stresses) were considered in the total strain energy density function. Therefore, the total strain energy, U, for a deformed isotropic linear elastic body occupying region Ω is given by

$$U = \frac{1}{2}\int_{\Omega}\left(\sigma_{ij}\varepsilon_{ij} + m_{ij}\chi_{ij}\right)dv \qquad (i, j = 1, 2, 3)$$

(1)

with the stress tensor, σ_{ij}, strain tensor, ε_{ij}, deviatoric part of the couple stress tensor, m_{ij}, and symmetric curvature tensor, χ_{ij}, are, respectively, defined by

$$\sigma_{ij} = \lambda tr\left(\varepsilon_{ij}\right)I + 2\mu\varepsilon_{ij} \tag{2}$$

$$\varepsilon_{ij} = \frac{1}{2}\left[\nabla u_i + \left(\nabla u_i\right)^T\right] \tag{3}$$

$$m_{ij} = 2l^2\mu\chi_{ij} \tag{4}$$

$$\chi_{ij} = \frac{1}{2}\left[\nabla\theta_i + \left(\nabla\theta_i\right)^T\right] \tag{5}$$

where λ and μ being Lame's constants, l a material length scale parameter, u_i the components of displacement vector and θ_i the components of rotation vector given by

$$\theta_i = \frac{1}{2}curl(u_i) \tag{6}$$

Obviously, both σ_{ij} and m_{ij}, as respectively defined in Eqs. (2) and (4), are symmetric, with $\sigma_{ij} = \sigma_{ij}^T$ and $m_{ij} = m_{ij}^T$ due to the symmetry of strain tensor and curvature tensor, ε_{ij} and χ_{ij}, given in Eqs. (3) and (5), respectively. The additional parameter l is regarded as a material property characterizing the effect of couple stresses initiated due to the micro-rotations.

3- Structural and Dynamical models of NWs based on MCST

The Cartesian axes for plane NW analysis are established, as shown in figure 2-1. The origin is placed at the bottom section. The total length of the NW was assumed to be L. As it will be shown in the following chapters, chapter 4, the GaN NWs have high aspect ratios, length to diameter ratio. Thus, the GaN NWs can be considered as Bernoulli-Euler beams.
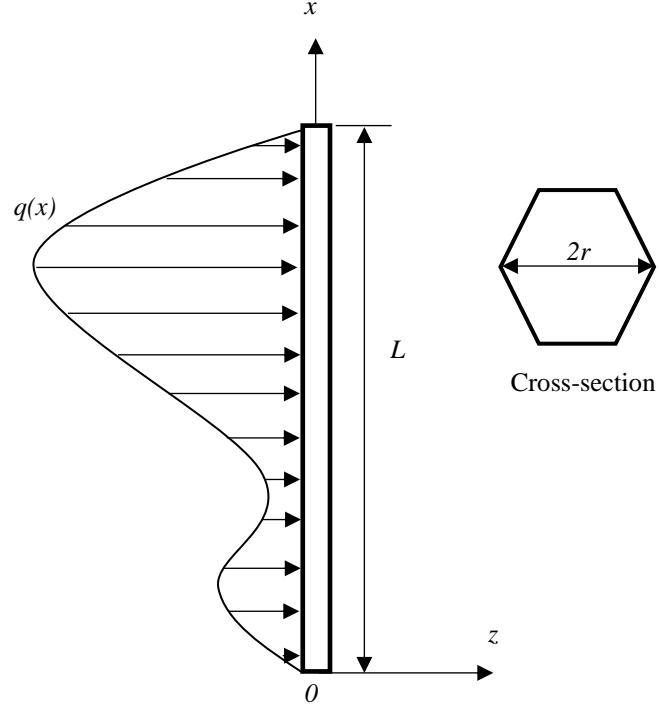
Figure 2-1: schematic picture of deformed GaN NWs under a general loading.

According to the basic hypotheses of the Bernoulli-Euler beams and the one-dimensional

beam theory, the displacement field at each point of the GaN NWs can be written as

$$u = -z\psi(x,t) \qquad \upsilon = 0 \qquad w = w(x,t) \tag{7}$$

where u, υ, w are the $x-$, $y-$, and $z-$components of the displacement vector, and

$\psi(x)$ is the rotation angle of the centroidal axis of the NWs. For infinitesimal

deformations, the rotation angle of the NWs can be approximated by

$$\psi(x) \approx \frac{\partial w(x,t)}{\partial x} \tag{8}$$

From Eqs. (3), (7) and (8), one can obtain

$$\varepsilon_{xx} = -z\frac{\partial^2 w(x,t)}{\partial x^2} \tag{9}$$

$$\varepsilon_{yy} = \varepsilon_{zz} = \varepsilon_{xy} = \varepsilon_{yz} = \varepsilon_{zx} = 0$$

And from Eqs. (6) to (8), it follows that

$$\theta_y = -\frac{\partial w(x,t)}{\partial x} \qquad \theta_x = \theta_z = 0 \tag{10}$$

The substituting Eq. (10) into Eq. (5) results in

$$\chi_{xy} = -\frac{1}{2}\frac{\partial^2 w(x,t)}{\partial x^2} \qquad \chi_{xx} = \chi_{yy} = \chi_{zz} = \chi_{xz} = \chi_{yz} = 0 \tag{11}$$

For a slender NW with a large aspect ratio, the Poisson's effect can be ignored to simplify the formulation of beam theory for the NW. Therefore, inserting Ep. (9) into Eq.

$$\sigma_{xx} = -Ez\frac{\partial^2 w}{\partial x^2} \qquad \sigma_{yy} = \sigma_{zz} = \sigma_{yz} = \sigma_{xz} = \sigma_{xy} = 0 \tag{12}$$

(2), yields

where E, v are respectively Young's modulus and the Poisson's ratio of the GaN NW. Similarly, the substitution of Eq. (11) into Eq. (4) leads to

$$m_{xy} = -\mu l^2 \frac{\partial^2 w}{\partial x^2} \qquad m_{xx} = m_{yy} = m_{zz} = m_{yz} = m_{xz} = 0 \tag{13}$$

where μ is the shear modulus defined as $\mu = \dfrac{E}{2(1+v)}$. Using Eqs. (9), (11), (12) and (13)

in Eq. (1) gives

$$U = \frac{1}{2}\int_0^L \left(EI + \mu Al^2\right)\left(\frac{\partial^2 w}{\partial x^2}\right)^2 dx \tag{14}$$

where I is the second moment of the cross-sectional and A is the area of the cross-sectional of the GaN NW. On the other hand, the work done by the external forces in the most general form of loading $q(x,t)$, as shown in figure 2-1, is

$$V = \int_0^L q(x,t)w(x,t)dx \tag{15}$$

On the other hand, the kinetic energy can be defined as

$$T = \frac{1}{2}\int_0^L \rho(x)A(x)\left(\frac{\partial w(x,t)}{\partial t}\right)^2 dx \tag{16}$$

where $\rho(x)$ is the density of the GaN NWs. At this point, the Hamilton's principle can be used to determine the dynamic governing equations of GaN NWs in the scope of MCST as well as all possible boundary conditions as follows

$$\delta\left\{\int_{t_1}^{t_2}(T-V-U)dt\right\}=0 \tag{17}$$

Inserting Eqs. (14)- (16) into Eq. (17) gives

$$\delta\int_{t_1}^{t_2}\int_0^L\left[\frac{1}{2}\rho A(\dot{w})^2 - \frac{1}{2}\left(EI + \mu Al^2\right)(w'')^2 + qw\right]dxdt = 0 \tag{18}$$

Where the Lagrange's function is

$$F = \frac{1}{2}\rho A(\dot{w})^2 - \frac{1}{2}\left(EI + \mu Al^2\right)(w'')^2 + qw \tag{19}$$

where

$$\dot{w} = \frac{\partial w(x,t)}{\partial t} \qquad w' = \frac{\partial w(x,t)}{\partial x} \qquad w'' = \frac{\partial^2 w(x,t)}{\partial x^2} \tag{20}$$

Implementing the calculus of variations, Eq. (18) can be expanded as

$$\delta \int_{t_1}^{t_2} \int_0^L \left[\frac{1}{2} \rho A (\dot{w})^2 - \frac{1}{2} \left(EI + \mu Al^2 \right) (w'')^2 + qw \right] dxdt$$

$$= \int_{t_1}^{t_2} \int_0^L \delta F (w'', w, \dot{w}) dxdt$$

$$= \int_{t_1}^{t_2} \left\{ \int_0^L \left[\frac{\partial^2}{\partial x^2} \left(\frac{\partial F}{\partial w''} \right) + \frac{\partial F}{\partial w} - \frac{\partial}{\partial t} \left(\frac{\partial F}{\partial \dot{w}} \right) \right] \delta w dx \right\} dt \tag{21}$$

$$+ \int_{t_1}^{t_2} \left[-\frac{\partial}{\partial x} \left(\frac{\partial F}{\partial w''} \right) \delta w + \frac{\partial F}{\partial w''} \delta w' \right]_0^L dt + \int_0^L \left(\frac{\partial F}{\partial \dot{w}} \delta w \right)_{t_1}^{t_2} dx$$

Substituting Eq. (19) into Eq. (21), the variational equation (21) takes the form

$$\int_{t_1}^{t_2} \int_0^L \left[-\left(EI + \mu Al^2 \right) w^{(4)} - \rho A \ddot{w} + q \right] \delta w dxdt - \int_{t_1}^{t_2} \left[\left(EI + \mu Al^2 \right) w^{(3)} \delta w \right]_0^L dt \tag{22}$$

$$- \int_{t_1}^{t_2} \left[\left(EI + \mu Al^2 \right) w'' \delta w' \right]_0^L dt + \int_0^L \left[\dot{w} \delta w \right]_{t_1}^{t_2} dx = 0$$

where

$$w^{(4)} = \frac{\partial^4 w}{\partial x^4} \qquad w^{(3)} = \frac{\partial^3 w}{\partial x^3} \qquad \ddot{w} = \frac{\partial^2 w}{\partial t^2} \tag{23}$$

In view of the Eq. (22), the dynamic governing equation of the NW in terms of $w(x,t)$ is

given by

$$\rho A \ddot{w} + EI w^{(4)} + \mu Al^2 w^{(4)} = q \tag{24}$$

the initial conditions as

$$\dot{w}(x,t_2) \delta w(x,t_2) - \dot{w}(x,t_1) \delta w(x,t_1) = 0 \tag{25}$$

and the equations

$$\left. \frac{\partial^2 w}{\partial x^2} \right|_{x=0,L} = 0 \qquad or \qquad \left. \frac{\partial w}{\partial x} \right|_{x=0,L}$$

$$\left. \frac{\partial^3 w}{\partial x^3} \right|_{x=0,L} = 0 \qquad or \qquad w \big|_{x=0,L} \tag{26}$$

prescribed at $x = 0$ and $x = L$ as the boundary conditions.

It can be seen from Eq. (24) that the governing equation of the NWs has two parts: one related to ρA and EI as in CCT and the other related to $\mu A l^2$. Moreover, it should be emphasized that the MCST contains only one additional material constants besides two classical material parameters. Nevertheless, the presence of l enables the incorporation of the GaN size features in the MCST and renders it possible to explain the size-effects of GaN NWs by taking into account the micro-rotations, couple stresses. It must be noted, letting $l = 0$, the MCST will reduce to the CCT.

4- Analysis of the GaN NWs using MCST

During the experiment, I applied a lateral infinitesimal deflection on the free end of the GaN NWs using AFM's tip while I was monitoring the normal deflection of the AFM's tip during loading and unloading cycles. Figure 2-2 shows the loading condition on each GaN NW in contact with the AFM's tip.
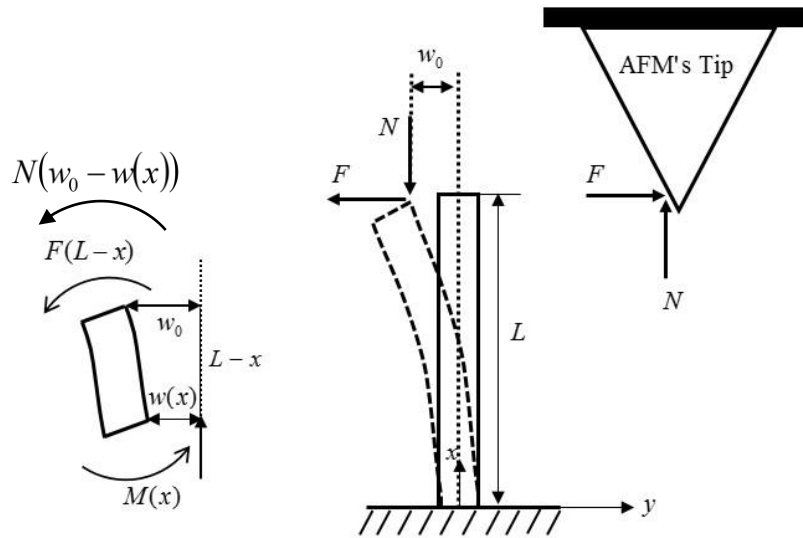
Figure 2-2: GaN NWs under loading.

The AFM's tip applies an axial force and a lateral force on the free end of the GaN NW. The moment equilibrium condition at any cross-section along the GaN NW can be written as

$$\sum M = 0 \quad \Rightarrow \quad M(x) = F(L-x) + N(w_0 - w) \tag{27}$$

where w_0, F, N and L are the maximum deflection at the free end of the GaN NW, $w|_{x=L} = w_0$, the lateral force, the normal force and the length of the nanowire, respectively. The total moment at each cross-section can be related to the deflection of the GaN NW as

$$M = \left(EI + \mu A l^2\right)\frac{d^2 w}{dx^2} \tag{28}$$

It should be emphasized that the distributed force, $q(x)$, is zero in this case because the AFM tip only touches the free end of each GaN NW. Furthermore, all partial derivatives respect to time are zero because the loading is stationary. Therefore, it gives

$$\left(EI + \mu A l^2\right)\frac{d^2 w}{dx^2} + Nw = Nw_0 + F(L-x) \tag{29}$$

Here, I have second-order nonhomogeneous linear differential equation. Therefore, the solution of this equation is summation of its both solutions, general solution, w_g, and particular solution, w_p. The general solution can be easily defined by considering the right-hand side of the above equation equal zero as follows

$$w_g = a\sin(kx) + b\cos(kx) \tag{30}$$

And the particular solution will be obtained as

$$w_p = w_0 + \frac{F}{N}(L-x) \tag{31}$$

Therefore,

$$w(x) = w_g + w_p = a\sin(kx) + b\cos(kx) + w_0 + \frac{F}{N}(L - x) \tag{32}$$

where k is the square root of the normal force to the rigidity of the nanowire ratio,

$$k = \sqrt{N \big/ \left(EI + \mu Al^2\right)}.$$

The unknown coefficients, a, b and w_0, can be determined using the boundary conditions. I assumed clamped boundary conditions, at the fixed end since the contact between the GaN NWs and the substrate is covalent type GaN-GaN bonds. Consequently, the NWs and the substrate are perfectly lattice matched, and there are not any stress concentrations at the fixed end. Furthermore, the SEM images were taken from a GaN NW while a nanomanipulator, also called omniprobe, was bending the GaN NW, figure 2-3. Figure 2-3 shows a strong connection between the substrate and the GaN NWs in the which validates the clamped boundary condition.
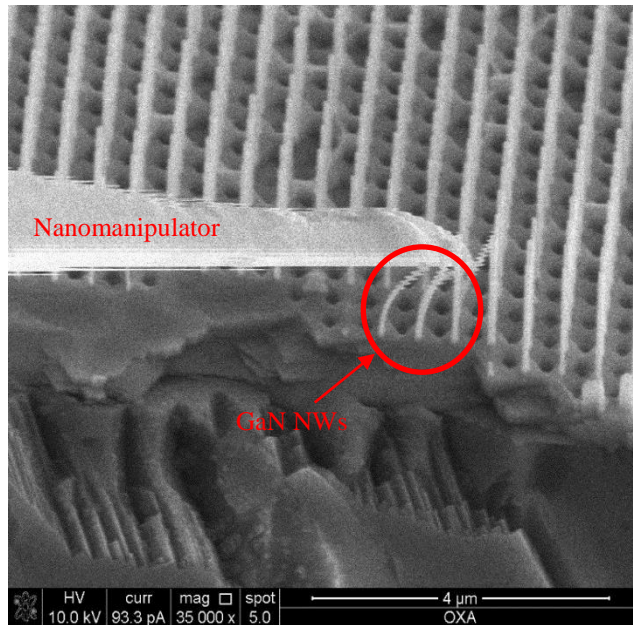
Figure 2-3: validating the clamped boundary conditions of the GaN NWs.

Therefore, the clamped boundary conditions at the fixed end are

$$w|_{x=0} = 0$$
$$\left.\frac{dw}{dx}\right|_{x=0} = 0$$

(34)

Furthermore, since we assumed w_0 to be the maximum deflection at the free end of GaN NWs, therefore

$$w|_{x=L} = w_0$$

(35)

Applying the above boundary conditions to the solution of the governing equation and simplifying the result is

$$w_0 = \frac{F}{N}\left(\frac{\tan(kL)}{k} - L\right)$$

(36)

In the above equation, we have the lateral force and normal force exerting on the nanowires while the AFM gives us only the normal force, equivalently, the normal deflection of the AFM's tip. However, one can easily find this ratio by considering the equilibrium conditions for the AFM's tip during the loading and unloading, for more information see chapter 5.

Chapter 3: Strain Gradient Theory

1- Introduction

In this chapter, a rigorous method for deriving the governing equations of the MSGT based on energy principle theory is presented. More details about the procedure for deriving the governing equations can be found in [65, 68-69]. After the rederiving the governing equations for MSGT, I solved the governing equation for the case of GaN NWs to derive the relationship between the deflection and force for each individual GaN NWs.

2- The MSGT for elasticity

A new version of the MSGT was proposed by Lam et al. [65], in which a new additional equilibrium equation to predict the behavior of higher-order stresses, the equilibrium of moments of couples, are introduced in additional to the classical equilibrium equations of forces and moments of forces [68]. In the governing equations of this theory, there are three independent higher-order materials length scale parameters associated with the higher strain gradients in addition to two classical material parameters for isotropic linear elastic materials. Then the total strain energy, U, of a deformable isotropic linear

$$U = \frac{1}{2}\int_{\Omega}\left(\sigma_{ij}\varepsilon_{ij} + p_i\gamma_i + \tau_{ijk}^{(1)}\eta_{ijk}^{(1)} + m_{ij}^s\chi_{ij}^s\right)dv \qquad (1)$$

elastic material occupying region Ω is given by

where the classical strain tensor and the higher gradients of the strain tensor are defined as follows,

$$\varepsilon_{ij} = \left(\partial_i u_j + \partial_j u_i \right) \tag{2}$$

$$\varepsilon_{mm,i} = \gamma_i = \partial_i \varepsilon_{mm} \tag{3}$$

$$\eta_{ijk}^{(1)} = \frac{1}{3} \left(\partial_i \varepsilon_{jk} + \partial_j \varepsilon_{ki} + \partial_k \varepsilon_{ij} \right) - \frac{1}{15} \delta_{ij} \left(\partial_k \varepsilon_{mm} + 2\partial_m \varepsilon_{mk} \right)$$
$$- \frac{1}{15} \left[\delta_{jk} \left(\partial_i \varepsilon_{mm} + 2\partial_m \varepsilon_{mi} \right) + \delta_{ki} \left(\partial_j \varepsilon_{mm} + 2\partial_m \varepsilon_{mj} \right) \right] \tag{4}$$

$$\chi_{ij}^s = \frac{1}{2} \left(e_{ipq} \partial_p \varepsilon_{qj} + e_{jpq} \partial_p \varepsilon_{qi} \right) \tag{5}$$

where ∂_i is differential operator, u_i is the displacement vector, ε_{ij} is the classical strain tensor, $\varepsilon_{mm,i}$ is the dilatation gradient vector, $\eta_{ijk}^{(1)}$ is the deviatoric stretch gradient tensor, χ_{ij}^s is the symmetric rotation gradient tensor, δ_{ij} and e_{ijk} are the Knocker delta and the alternate tensor. It should be mentioned, in the above and in subsequent equations, the index notation will be used with repeated indices rendering summation from 1 to 3. Moreover, the corresponding classical and non-classical stress tensors are defined as follows

$$\sigma_{ij} = k\delta_{ij}\varepsilon_{mm} + 2\mu\varepsilon_{ij}' \tag{6}$$

$$p_i = 2\mu l_0^2 \gamma_i \tag{7}$$

$$\tau_{ijk}^{(1)} = 2\mu l_1^2 \eta_{ijk}^{(1)} \tag{8}$$

$$m_{ij}^s = 2\mu l_2^2 \chi_{ij}^s \tag{9}$$

where ε_{ij}' is deviatoric strain tensor introduced as

$$\varepsilon_{ij}' = \varepsilon_{ij} - \frac{1}{3}\varepsilon_{mm}\delta_{ij} \tag{10}$$

where k and μ are bulk and shear module, respectively, and l_0, l_1, l_2 are additional independent material parameters associated with dilatation gradients, deviatoric stretch gradients and rotation gradient for the GaN NWs, respectively.

3- Structural and dynamical models of NWs based on MSGT

According to the energy principle theory, the governing equation of a NW under any general form of loading as well as all boundary conditions can be determined with the aid of a variational principle [46]

$$\delta(U - W) = 0 \tag{11}$$

where U is the total strain energy and W is the total work done by external forces and δ indicates variation. Figure 3-1 shows an uniform GaN NW, which is subjected to a general loading distribution, $q(x)$, along its longitudinal axis x. Hence, the loading plane coincides with the xz plane, and the cross-section of the beam parallel to the yz plane.
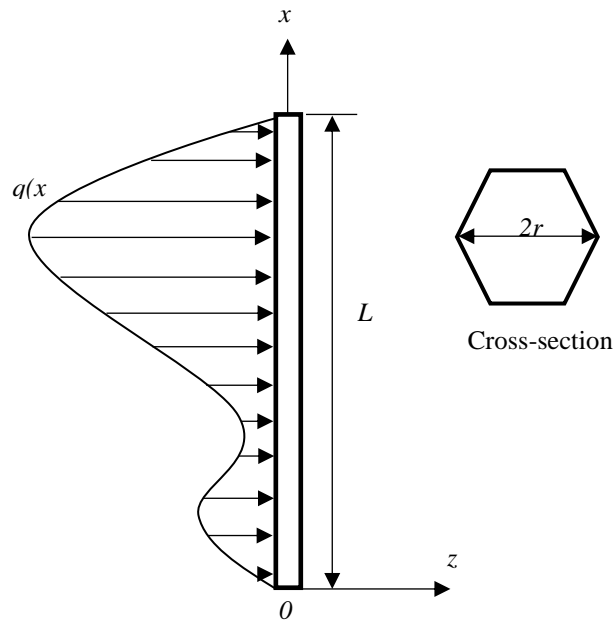
Figure 3-1: a NW under general form of lateral force.

Similar to the previous section, because the aspect ratios, length to diameter ratio, of GaN NWs are large, we can model them as Bernoulli-Euler beam. According to the Bernoulli-Euler hypothesis and the one-dimensional beam theory, the displacement field of a GaN NW in bending can be written as

$$u = -z\frac{\partial w(x)}{\partial x} \qquad v = 0 \qquad w = w(x) \tag{12}$$

where u, v, w, are the $x-$, $y-$, and $z-$components of the displacement vector, respectively. Inserting Eq. (12) into Eq. (2), then the classical strain tensor can be determined, where the only non-zero strain component is

$$\varepsilon_{xx} = -z\frac{\partial^2 w}{\partial x^2} \tag{13}$$

And from Eqs. (2) and (3) it follows that

$$\gamma_x = -z\frac{\partial^3 w}{\partial x^3} \qquad \gamma_y = 0 \qquad \gamma_z = -\frac{\partial^2 w}{\partial x^2} \tag{14}$$

By using Eq. (2) in Eq. (5) gives the stretch gradient tensor, where the only non-zero stretch gradients, χ_{ij}^s, components are

$$\chi_{xy}^s = \chi_{yx}^s = -\frac{1}{2}\frac{\partial^2 w}{\partial x^2} \tag{15}$$

By substituting Eq. (2) into Eq. (4), the non-zero dilatation gradients, $\eta_{ijk}^{(1)}$, can be found as

$$\eta_{111}^{(1)} = -\frac{2}{5}z\frac{\partial^3 w}{\partial x^3} \qquad \eta_{113}^{(1)} = -\frac{4}{15}\frac{\partial^2 w}{\partial x^2} \qquad \eta_{122}^{(1)} = \frac{1}{5}z\frac{\partial^3 w}{\partial x^3}$$

$$\eta_{133}^{(1)} = \frac{1}{5}z\frac{\partial^3 w}{\partial x^3} \qquad \eta_{212}^{(1)} = \frac{1}{5}z\frac{\partial^3 w}{\partial x^3} \qquad \eta_{111}^{(1)} = \frac{1}{5}z\frac{\partial^3 w}{\partial x^3}$$

$$\eta_{223}^{(1)} = \frac{1}{15}\frac{\partial^2 w}{\partial x^2} \qquad \eta_{232}^{(1)} = \frac{1}{15}\frac{\partial^2 w}{\partial x^2} \qquad \eta_{111}^{(1)} = -\frac{4}{15}\frac{\partial^2 w}{\partial x^2}$$

$$\eta_{313}^{(1)} = \frac{1}{5}z\frac{\partial^3 w}{\partial x^3} \qquad \eta_{322}^{(1)} = \frac{1}{15}\frac{\partial^2 w}{\partial x^2} \qquad \eta_{331}^{(1)} = \frac{1}{5}z\frac{\partial^3 w}{\partial x^3} \qquad \eta_{333}^{(1)} = \frac{1}{5}\frac{\partial^2 w}{\partial x^2}$$

(16)

It can be concluded from Eq. (10) and (13) that

$$\varepsilon_{xx}' = \frac{2}{3}\varepsilon_{xx} \qquad \varepsilon_{yy}' = \varepsilon_{zz}' = -\frac{1}{3}\varepsilon_{xx}$$

(17)

For a slender beam with a large aspect ratio, the Poisson effect is secondary and may be neglected to facilitate the formulation of a simple beam theory. By considering $v = 0$, as was done in CCT, inserting Eqs. (13) and (17) into Eq. (6) then gives the non-zero classical stresses σ_{ij} as

$$\sigma_{xx} = E\varepsilon_{xx} = -Ez\frac{\partial^2 w}{\partial x^2}$$

(18)

The use of Eq. (14) in Eq. (7) gives

$$p_x = -2\mu l_0^2 z\frac{\partial^3 w}{\partial x^3} \qquad p_y = 0 \qquad p_z = -2\mu l_0^2\frac{\partial^2 w}{\partial x^2}$$

(19)

and by inserting Eq. (15) into Eq. (9), the only non-zero higher-order stress m_{ij}^s is

$$m_{ij}^s = m_{xy}^s = 2\mu l_2^2\left(-\frac{1}{2}\frac{\partial^2 w}{\partial x^2}\right) = -\mu l_2^2\frac{\partial^2 w}{\partial x^2}$$

(20)

Similarly, from Eqs. (16) and (8), the non-zero higher-order stresses $\tau_{ijk}^{(1)}$ are

$$
\begin{aligned}
&\tau_{111}^{(1)} = -\frac{4}{5}\mu l_1^2 z \frac{\partial^3 w}{\partial x^3} && \tau_{113}^{(1)} = -\frac{8}{15}\mu l_1^2 \frac{\partial^2 w}{\partial x^2} && \tau_{122}^{(1)} = \frac{2}{5}\mu l_1^2 z \frac{\partial^3 w}{\partial x^3} \\
&\tau_{133}^{(1)} = \frac{2}{5}\mu l_1^2 z \frac{\partial^3 w}{\partial x^3} && \tau_{212}^{(1)} = \frac{2}{5}\mu l_1^2 z \frac{\partial^3 w}{\partial x^3} && \tau_{111}^{(1)} = \frac{2}{5}\mu l_1^2 z \frac{\partial^3 w}{\partial x^3} \\
&\tau_{223}^{(1)} = \frac{2}{15}\mu l_1^2 \frac{\partial^2 w}{\partial x^2} && \tau_{232}^{(1)} = \frac{2}{15}\mu l_1^2 \frac{\partial^2 w}{\partial x^2} && \tau_{111}^{(1)} = -\frac{8}{15}\mu l_1^2 \frac{\partial^2 w}{\partial x^2} \\
&\tau_{313}^{(1)} = \frac{2}{5}\mu l_1^2 z \frac{\partial^3 w}{\partial x^3} && \tau_{322}^{(1)} = \frac{2}{15}\mu l_1^2 \frac{\partial^2 w}{\partial x^2} && \tau_{331}^{(1)} = \frac{2}{5}\mu l_1^2 z \frac{\partial^3 w}{\partial x^3} && \tau_{333}^{(1)} = \frac{2}{5}\mu l_1^2 \frac{\partial^2 w}{\partial x^2}
\end{aligned}
\tag{21}
$$

Substituting Eqs. (13) - (15), (16), (19), (21) into Eq. (1), the following expression can be achieved for the total strain energy U

$$
U = \frac{1}{2}\int_0^L \left[S.(w'')^2 + K.(w^{(3)})^2 \right]
\tag{22}
$$

where

$$
K = I\left(2\mu l_0^2 + \frac{4}{5}\mu l_1^2 \right) \qquad S = EI + 2\mu A l_0^2 + \frac{43}{225}\mu A l_1^2 + \mu A l_2^2
\tag{23}
$$

$$
w'' = \frac{\partial^2 w}{\partial x^2} \qquad w^{(3)} = \frac{\partial^3 w}{\partial x^3}
$$

and I is the inertia moment of the cross-section and A is the area of the cross section of the GaN NW.

Taking the first variation of Eq. (22) results in, together with Eq. (23)

$$
\begin{aligned}
\delta U &= \delta \int_0^L F\left(w'', w^{(3)} \right) dx \\
&= \int_0^L \left[\frac{d^2}{dx^2}\left(\frac{\partial F}{\partial w''} \right) - \frac{d^3}{dx^3}\left(\frac{\partial F}{\partial w^{(3)}} \right) \right] \delta w \, dx + \left[\left(-\frac{d}{dx}\left(\frac{\partial F}{\partial w''} \right) + \frac{d^2}{dx^2}\left(\frac{\partial F}{\partial w^{(3)}} \right) \right) \delta w \right]_0^L \\
&\quad \left[\left(\left(\frac{\partial F}{\partial w''} \right) - \frac{d}{dx}\left(\frac{\partial F}{\partial w^{(3)}} \right) \right) \delta w' \right]_0^L + \left[\frac{\partial F}{\partial w^{(3)}} \delta w'' \right]_0^L
\end{aligned}
\tag{24}
$$

where, the Lagrangian function, F, is

$$F = \frac{1}{2}\left[S.(w'')^2 + K.\left(w^{(3)}\right)^2\right]$$ (25)

Eqs. (24) and (25) can be utilized to represent the variation of the total strain energy of the GaN NWs as

$$\delta U = \int_0^L \left[S.w^{(4)} - K.w^{(6)}\right]\delta w\,dx + \left[-S.w^{(3)} + K.w^{(5)}\right]\delta w\Big|_0^L + \left[S.w'' - K.w^{(4)}\right]\delta w'\Big|_0^L + K.w^{(3)}\,\delta w''\Big|_0^L$$ (26)

where

$$w' = \frac{\partial w}{\partial x} \qquad w^{(4)} = \frac{\partial^4 w}{\partial x^4} \qquad w^{(5)} = \frac{\partial^5 w}{\partial x^5} \qquad w^{(6)} = \frac{\partial^6 w}{\partial x^6}$$ (27)

On the other hand, the variation of the work done by the external forces, $q(x)$, the boundary shear force, V, and the boundary classical and non-classical bending moments, M and M^h, respectively, reads

$$\delta V = \int_0^L q(x)\delta w(x)\,dx + \left[V\delta w\right]_0^L + \left[M\delta w'\right]_0^L + \left[M^h\delta w''\right]_0^L$$ (28)

In view of Eqs. (26) and (28), the variational form of Eq. (11) takes the form

$$\delta(U - V) = \int_0^L \left[S.w^{(4)} - K.w^{(6)} - q\right]\delta w\,dx + \left[-S.w^{(3)} + K.w^{(5)} - V\right]\delta w\Big|_0^L$$
$$+ \left[S.w'' - K.w^{(4)} - M\right]\delta w'\Big|_0^L + \left[K.w^{(3)} - M^h\right]\delta w''\Big|_0^L = 0$$ (29)

The above variational equation implies that each term must be equal to zeros. Hence, the governing equation of the GaN NWs in bending is given by

$$S.w^{(4)} - K.w^{(6)} - q = 0$$ (30)

while the boundary conditions must satisfy the following equations

$$\left[V(L)-\left[K.w^{(5)}(L)-S.w^{(3)}(L)\right]\right]\delta w(L)-\left[V(0)-\left[K.w^{(5)}(0)-S.w^{(3)}(0)\right]\right]\delta w(0)=0$$
$$\left[M(L)-\left[K.w''(L)-S.w^{(4)}(L)\right]\right]\delta w'(L)-\left[M(0)-\left[K.w''(0)-S.w^{(4)}(0)\right]\right]\delta w'(0)=0 \qquad (31)$$
$$\left[M^{h}(L)-K.w^{(3)}(L)\right]\delta w''(L)-\left[M^{h}(0)-K.w^{(3)}(0)\right]\delta w''(0)=0$$

For boundary conditions, if one assumes the four classical boundary conditions to be $w(0)$, $w(L)$, $w'(0)$ and $w'(L)$ prescribed and the corresponding non-classical ones to be $w''(0)$ and $w''(L)$ prescribed, then $\delta w(0)=\delta w(L)=0$, $\delta w'(0)=\delta w'(L)=0$, $\delta w''(0)=\delta w''(L)=0$ and Eq. (31) are all satisfied. In virtue of Eq. (31), one can get that, when dealing with the classical boundary conditions, either the deflection w or the boundary shear forces $V=Kw^{(5)}-Sw^{(3)}$ and the strain, w', or the boundary classical bending moments $M=Sw''-Kw^{(4)}$ at the boundaries of the beam must be specified. For the case of the non-classical boundary conditions, one must specify either the boundary strain gradient, w'', or the non-classical boundary moments as $M^{h}=Kw^{(3)}$.

It should be mentioned, when the higher-order material parameters l_0 and l_1 equal to zero, then the constitutive relation reduces to that of the MCST and the corresponding governing equation reads

$$\left[V(L)+\left(EI+\mu Al_2^2\right)w^{(3)}(L)\right]\delta w(L)-\left[V(0)+\left(EI+\mu Al_2^2\right)w^{(3)}(0)\right]\delta w(0)=0$$
$$\left[M(L)-\left(EI+\mu Al_2^2\right)w''(L)\right]\delta w'(L)-\left[M(0)-\left(EI+\mu Al_2^2\right)w''(0)\right]\delta w'(0)=0 \qquad (32)$$

There results conform to solutions based on the MCST [48]. Moreover, when all three higher-order material parameters, e.g. l_0, l_1, l_2, equal to zero, then the constitutive relation reduces to that of the CCT.

4- Solution for the GaN NWs using MSGT

Before defining the solution of the above equations, we need to determine our assumptions. Figure 3-2 shows the nanowire under loading during the experiment. The center of the Cartesian coordinate system is fixed at the clamped end, where the nanowires are connected to the substrate.
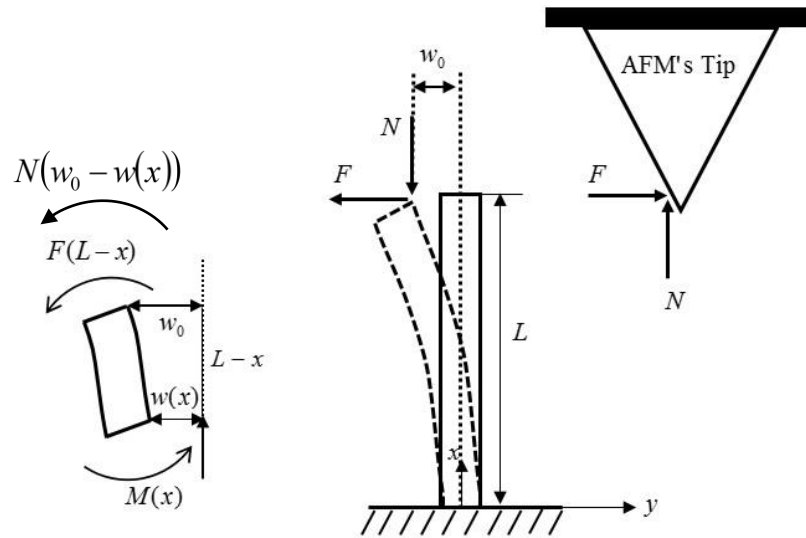
Figure 3-2: schematically showing the deformation of the GaN NWs under loading.

To solve the governing equation of the MSGT, the first assumptions are the steady state process, static process, therefore, the time derivatives are zero. Furthermore, there is not any distributed lateral loading, $q(x)=0$. Writing the equilibrium condition for the total moment at any point along the NW reads

$$\sum M = 0 \quad \Rightarrow \quad M(x) = F(L-x) + N(w_0 - w) \tag{33}$$

The total moment at any point is related to the external distributed load as

$$M(x) = -\int_0^L \int_0^L q(x)dxdx \tag{34}$$

which is related to the deflection of the beam as follows

$$M(x) = \int_0^L \int_0^L q(x)dxdx = \left(S\frac{d^2w}{dx^2} - K\frac{d^4w}{dx^4} \right) \tag{35}$$

Substituting Eq. (35) into Eq. (30) and rearranging leads to

$$S\frac{d^2w}{dx^2} - K\frac{d^4w}{dx^4} + Nw = Nw_0 + F(L-x) \tag{36}$$

Eq. (36) is a second-order, linear and nonhomogeneous differential equation, which its solution is summation of the general solution, w_g, and the particular solution, w_p. To find the general solution, one must consider its homogenous form to determine the characteristic equation of the differential equation. To do so, since all coefficients are constants, then I consider the solution as an exponential equation, $\exp(\lambda x)$, therefore the characteristic equation will be found

$$J\lambda^4 - \lambda^2 - P = 0 \tag{37}$$

where J and P are constants equal to $J = K/S$ and $P = N/S$. Noted that both J and P are positive, which leads in four solutions, two pure real solutions and two pure imaginary solutions as

$$
\begin{aligned}
\lambda_1^2 &= \frac{1 + \sqrt{1+4JP}}{2J} > 0 \quad &\rightarrow \quad \lambda_1 &= \sqrt{\frac{\sqrt{1+4JP}+1}{2J}} \\
\lambda_2^2 &= \frac{1 - \sqrt{1+4JP}}{2J} < 0 \quad &\rightarrow \quad \lambda_2 &= j\sqrt{\frac{\sqrt{1+4JP}-1}{2J}}
\end{aligned}
\tag{38}
$$

Therefore, the general solution for Eq. (36) will be

$$w_g(x) = a\sin(\lambda_2 x) + b\cos(\lambda_2 x) + c\sinh(\lambda_1 x) + d\cosh(\lambda_1 x) \tag{39}$$

Considering the Eq. (36), the particular solution can be demonstrated as

$$w_p(x) = w_0 + \frac{F}{N}(L - x) \tag{40}$$

Finally, the solution for Eq. (36) determined by summation of Eqs. (39) and (40) solutions

is

$$w(x) = w_p(x) + w_g(x) = a\sin(\lambda_2 x) + b\cos(\lambda_2 x) \tag{41}$$
$$+ c\sinh(\lambda_1 x) + d\cosh(\lambda_1 x) + w_0 + \frac{F}{N}(L - x)$$

The classical and non-classical boundary conditions are

$$\begin{aligned}
&w(x = 0) = 0 \\
&w(x = L) = w_0 \\
&\frac{dw}{dx}(x = 0) = 0 \\
&\frac{d^3 w}{dx^3}(x = 0) = 0 \\
&\frac{d^3 w}{dx^3}(x = L) = 0
\end{aligned} \tag{42}$$

Applying the boundary conditions to the solution equation, the coefficients can be found

as

$$a = \frac{F}{N} \frac{\lambda_1^2}{\lambda_1^2 \lambda_2 + \lambda_2^3}$$

$$b \equiv B \frac{F}{N} = \frac{F}{N} \frac{\lambda_1^3 \sinh(\lambda_1 L)G - H \cos(\lambda_1 L)}{\lambda_1^3 \sinh(\lambda_1 L)\cos(\lambda_2 L) - \lambda_2^3 \cosh(\lambda_1 L)\sin(\lambda_2 L)}$$

$$c = \frac{F}{N} \frac{\lambda_2^2}{\lambda_2^2 \lambda_1 + \lambda_1^3}$$

$$d \equiv D \frac{F}{N} = \frac{F}{N} \frac{H \cos(\lambda_2 L) - \lambda_2^3 \sin(\lambda_2 L)G}{\lambda_1^3 \sinh(\lambda_1 L)\cos(\lambda_2 L) - \lambda_2^3 \cosh(\lambda_1 L)\sin(\lambda_2 L)}$$

$$G = -\left[\frac{\lambda_1^2}{\lambda_1^2 \lambda_2 + \lambda_2^3} \sin(\lambda_2 L) + \frac{\lambda_2^2}{\lambda_2^2 \lambda_1 + \lambda_1^3} \sinh(\lambda_1 L) \right]$$

$$H = \frac{\lambda_1^2 \lambda_2^2}{\lambda_1^2 + \lambda_2^2} \cos(\lambda_2 L) - \frac{\lambda_1^2 \lambda_2^2}{\lambda_1^2 + \lambda_2^2} \cosh(\lambda_1 L)$$

(43)

Substituting Eqs. (43) into Eq. (41), on can achieve

$$(B + D + L)\frac{F}{N} + w_0 = 0$$

(44)

In Eq. (42), the first three boundary conditions are the classical boundary conditions demonstrating the clamped boundary condition at the fixed end of the GaN NWs. The proof of the clamped boundary condition of the GaN NWs was provided in figure 2-3 of chapter 2.

Chapter 4: Theoretical Simulation Using Quantum Mechanics

1- Introduction

In this chapter, a theoretical method based on quantum mechanics theories for calculating the lattice dynamic matrix, or phonon band structure, has been provided to predict the mechanical properties of GaN NWs theoretically. In the first section, I explained the method for deriving the lattice dynamic matrix based on the solid mechanics framework, more details for this part can be found at [70-71]. Then, a brief explanation of deriving the dynamic matrix based on quantum mechanics theories is provided, more details for this part can be found at [71-72].

2- Lattice dynamic matrix based on solid mechanics

According to the linearized theory of a homogeneous elastic medium and considering the gradients of strains, a general form of the Lagrangian density, ψ, for a solid can be written as follows [71]

$$\psi = \frac{1}{2}\rho\dot{u}_i\dot{u}_i - \frac{1}{2}C_{ijkl}\varepsilon_{ij}\varepsilon_{kl} - D_{ijklm}u_{i,j}u_{k,lm} - F^1_{ijklmn}u_{i,jk}u_{l,mn} - F^2_{ijklmn}\varepsilon_{ij}u_{k,lmn} - ... \tag{1}$$

where ρ is the density, the ratio of the mass to volume, of the GaN, $\mathbf{u}$ is the displacement vector, the dot on top of displacement components stands for differentiation with respect to time and the comma stands for differentiation with respect to the spatial variables in the reference coordinate. The first term in the expression of the potential energy is due to the

long-wavelength elastic excitations of the solid, equivalently, the lowest-order description of sound wave propagation in the medium, which is GaN here.

Therefore, C_{ijkl} is the stiffness matrix defined in the CCT. In the bulk scales, the long-wavelength elastic excitations of the solid are the dominant terms in the potential energy while the higher-order strain gradients represented by non-classical terms, $\mathbf{D}$, $\mathbf{F^1}$ and $\mathbf{F^2}$, have a negligible contribution on the potential energy. However, in the nanoscales, where the strain gradients are comparable with dimensions of the nanostructure, the non-classical terms have significant effects. Lastly, $\boldsymbol{\varepsilon}$ is the strain tensor obtained using

$$\boldsymbol{\varepsilon} = \frac{1}{2}\left(\nabla \mathbf{u} + \left(\nabla \mathbf{u}\right)^T\right) \tag{2}$$

It is noteworthy to be mentioned that the Lagrangian density consists of the total kinetic energy and the potential energy, the first term shows the kinetic energy and the remaining terms are the potential energy. The potential energy density is invariant in the Euclidean group transforming. That is why the internal energy density only depends on the first- and higher-order derivatives of the displacement, not only on the displacement components. Invariance condition under the rigid rotations disregard the contribution of the asymmetric part of the strains and strain gradients on the internal energy density [71].

In order to derive the dynamical matrix of the GaN, one can use the variational analysis as demonstrated in [70]. Therefore, applying the variational principle leads to

$$\delta\left[\int \psi \, dx \, dt\right] = 0,$$

$$\int dx \int dt \left\{ \begin{array}{l} \rho \delta \ddot{u}_\alpha \dot{u}_\alpha - \dfrac{1}{2} C_{ijkl}\left[(\delta u_i)_{,j} u_{k,l} + (\delta u_k)_{,l} u_{i,j}\right] - D_{ijklm}\left[(\delta u_k)_{,l} u_{k,lm} + (\delta u_k)_{,lm} u_{i,j}\right] \\ - F^1_{ijklmn}\left[(\delta u_i)_{,j} u_{k,lmn} + (\delta u_k)_{,lmn} u_{i,j}\right] - F^1_{ijklmn}\left[(\delta u_i)_{,jl} u_{k,mn} + (\delta u_k)_{,mn} u_{i,j}\right] \\ - ... \end{array} \right\} \tag{3}$$

Implementing the integral by part technique onto Eq. (3), the dynamic governing equation can be obtained as

$$\rho \ddot{u}_i = c_{ijkl} u_{k,lj} + d_{ijklm} u_{k,lmj} + f_{ijklmn} u_{k,lmnj} + ... \tag{4}$$

To derive Eq. (4) from Eq. (3), the following constrains were applied.

$$\begin{aligned} c_{ijkl} &= sym_{(i,k)} sym_{(j,l)} C_{ijkl} \\ d_{ijklm} &= asym_{(i,k)} sym_{(j,l,m)} D_{ijklm} \\ f_{ijklmn} &= sym_{(i,k)} sym_{(j,l,m,n)}\left(F^2_{ijklmn} - F^1_{ijklmn}\right) \end{aligned} \tag{5}$$

where *sym* and *asym* symbols represent the symmetric and asymmetric parts of the elastic constant tensors respect to the indices mentioned as subscripts.

It should be emphasized that the fifth-order tensor **d** in Eq. (5) demonstrates an interesting phenomenon in the solid, named Acoustic Activity. The acoustic activities inside a solid are the same as the well-known phenomenon of optical activities which describe the effect of spatial dispersion on the propagation of an electromagnetic wave. The optical activities mainly contribute to first-order dispersive contributions to the dielectric constant tensor which is usually a function of the frequency only without dependency on the wave-vector [70]. In the optical activities, the dispersive effects can be fully explained by considering an invoking non-local dependence of the electric displacement vector **D** in an electric field, **E** . The same concept is also valid for the

acoustic activity in a solid. The fifth-order elastic tensor **d** in this description, is similar to the gyroscopic tensor in the optical activity, that it provides a first-order wave-vector dependence to the elastic tensor.

Eventually, to derive the lattice dynamic matrix, one can consider propagation of a plane-wave in the medium, with solution of the form of $u_i = u_i^0 \exp(i\omega t + i\mathbf{k.r})$, which results in

$$\rho\omega^2 u_i^0 = \left(c_{ijkl}k_jk_l + id_{ijklm}k_jk_lk_m - f_{ijklmn}k_jk_lk_mk_n + ...\right)u_k^0 \tag{6}$$

where the dynamic matrix, $R(k)$, is defined as

$$R(k) = c_{ijkl}k_jk_l + id_{ijklm}k_jk_lk_m - f_{ijklmn}k_jk_lk_mk_n + ... \tag{7}$$

Using the lattice dynamic matrix, one can easily calculate the phonon dispersion relations, which express the acoustic and optical frequencies in terms of wave-vector, for GaN. To do so, the eigenvalues of the equation must be calculated.

It is noteworthy to be mentioned that Eq. (7) renders the general form of the lattice dynamic matrix for a linear body. If one neglects the non-classical terms, the lattice dynamical matrix reduces to the CCT definition of the lattice dynamic matrix which is $c_{ijkl}k_jk_l$. Furthermore, to derive the non-classical properties of the GaN NWs according to the MCST or MSGT, the appropriate non-classical mechanical properties of the GaN must be considered and the remaining must be ignored.

3- Lattice dynamic matrix based on quantum mechanics

Several approaches for demonstrating the lattice dynamic matrix in the framework of the quantum mechanics have been proposed over the years, such as density functional perturbation, density functional theory, ab initio first principle, rigid valence shell model, rigid ion model, polarizable bond charges model and deformable ion model. Furthermore, there are some strong software available, such as Quantum ESPRESSO [73] or Atomic Tool Kit Virtual Nano-Lab (ATK-VNL) [74], that can be used to calculate the lattice dynamic matrix. In this thesis, I used the ATK-VNL to calculate the lattice dynamic matrix and phonon band structure of the GaN NWs. Therefore, I focus on linking the lattice dynamic matrix in the pure framework of the solid mechanics to the lattice dynamic matrix calculated in the pure quantum mechanics framework.

Comparing with the solid mechanics approach, from the microscopic lattice-dynamic viewpoint, the lattice dynamic matrix of a crystalline solid including more than one atom in its unit cell can be defined as [75]

$$R_{ik}^{\alpha\beta}(\mathbf{k}) = \frac{\rho}{\sqrt{M_\alpha M_\beta}} \sum_p K_{ik}^{\alpha p \beta q} \exp\left[i\mathbf{k}.\left(\mathbf{X}^{\beta q} - \mathbf{X}^{\alpha p}\right)\right] \tag{8}$$

where M_α and M_β are the masses of the α-th and β-th atoms, respectively. Furthermore, $K_{ik}^{\alpha p \beta q}$, $\mathbf{X}^{\beta q}$ and $\mathbf{X}^{\alpha p}$ are the atomic force constant matrixes, the position of the atom β in q-th unit cell and the position of the atom α in p-th unit cell, respectively. The long-wavelength limit ($k \rightarrow 0$) of Eq. (8) can be obtained by expanding $R(\mathbf{k})$ in powers of $\mathbf{k}$ until the first non-vanishing term to appear as

$$R(\mathbf{k}) = c'_{ijkl} k_j k_l \tag{9}$$

where the tensor $\mathbf{c}'$ can be found as

$$c'_{ijkl} = -\frac{1}{2\Omega_0} \sum_n K_{ik}^{mn} \left(\mathbf{X}^n - \mathbf{X}^m \right)_a \left(\mathbf{X}^n - \mathbf{X}^m \right)_b \tag{10}$$

The constants c'_{ijkl} have the same symmetry as the elastic constants c_{ijkl} of Eq. (5). Consequently, they are similar tensors. Regarding to this fact, the solid mechanics is sometimes referred to as a long-wavelength approximation of lattice-dynamical theory. Similarly, to identify microscopic material constants which resemble the elastic constants $\mathbf{d}$ and $\mathbf{f}$ of Eq. (7), one can easily approximate the equation to higher-orders of $\mathbf{k}$.

However, the identification between the discrete and continuum nature of the material is not so readily apparent when the crystal lattice ceases to be a Bravais lattice. Eq. (7) derived in the framework of the solid mechanics includes three governing equations for demonstrating the mechanical behaviors of a nanostructure in three dimensional spaces. On the other hand, Eq. (8) derived from a lattice-dynamical point of view includes $3N$ governing equations, where N is the number of atoms per unit cell. Three solutions to this eigenvalue problem posed by Eq. (10) correspond to acoustic phonons while the remaining $3(N-1)$ modes are the optical phonon modes.

4- Block diagonalizing the lattice dynamic matrix

The last step after calculating the lattice dynamic matrix using one of the quantum mechanics theories is to block diagonalize the lattice dynamic matrix. That is why the acoustic and optical phonons modes in the dynamic matrix are coupled, which they must

be decoupled. More details regarding to the block diagonalizing the lattice dynamic matrix can be found in [70].

At $\mathbf{k} = (0,0,0)$, also named Gamma point, a unitary transformation, U, can be implemented in order to block diagonalize the lattice dynamical matrix. Applying this unitary transformation matrix at the Gamma point results in

$$R^U(\mathbf{k}=0) = U^T R(\mathbf{k}=0)U = \begin{bmatrix} D_{3\times3}^a & 0_{3\times3} \\ 0_{3\times3} & D_{3\times3}^o \end{bmatrix} \tag{11}$$

where matrices $D_{3\times3}^a$ and $D_{3\times3}^o$ are the low frequencies, called acoustic modes, and high frequencies, called optical modes, respectively, contributions to the lattice dynamical matrix. The $D_{3\times3}^a$ is the dynamical matrix derived using the solid mechanics theory. However, for the case of $\mathbf{k} \neq 0$, applying the same unitary transformation matrix will not results in a full decoupled transformed matrix, there are acousto-optical coupling modes which must be decoupled.

$$R^U(\mathbf{k}) = U^T R(\mathbf{k})U = \begin{bmatrix} D_{3\times3}^a + O(\mathbf{k})\mathbf{I}_{3\times3} & O(\mathbf{k})\mathbf{I}_{3\times3} \\ O(\mathbf{k})\mathbf{I}_{3\times3} & D_{3\times3}^o + O(\mathbf{k})\mathbf{I}_{3\times3} \end{bmatrix} \tag{12}$$

This form of the lattice dynamical matrix is only valid if the used quantum mechanics model is analytical near the Gamma point. This constrain is not valid for the polar crystals whose Coulombic terms contributing to the lattice dynamical matrix have a macroscopic field term of the form $k_\alpha k_\beta / k^2$. However, for a slightly semi-polar and non-polar materials, the effect of the non-analyticity could be ignored [76]. Therefore, regarding to the analyticity of the lattice dynamic matrix, it is possible to find an orthogonal transformation in order to fully decouple the optical and acoustic modes. This well-known orthogonal transformation is Hermitian matrix. Thus,

$$\exp\left(-i\delta H\right)R^{U}\left(\mathbf{k}\right)\exp\left(i\delta H\right)=\begin{bmatrix} D_{3\times3}^{a} & 0_{3\times3} \\ 0_{3\times3} & D_{3\times3}^{o} \end{bmatrix} \tag{13}$$

Similar to [70], a perturbative approach can be employed to find δH. Moreover, the transformed lattice dynamic matrix can be approximated using a Taylor series as

$$\begin{bmatrix} D_{3\times3}^{aa} & 0_{3\times3} \\ 0_{3\times3} & D_{3\times3}^{oo} \end{bmatrix}=\sum_{j=0}^{\infty}K^{(j)} \tag{14}$$

where

$$K^{(0)}=H_{0}, \ K^{(1)}=Y, \ K^{(2)}=\frac{1}{2}\left[X^{H},X\right], \ K^{(3)}=\frac{1}{2}\left[X,\left[Y,X^{H}\right]^{H}\right]$$

$$K^{(4)}=\frac{1}{2}\left[X,\left\{\left[\left[Y,X^{H}\right]^{H},Y\right]^{H}+\frac{2}{3}\left[K^{(2)},X^{H}\right]^{H}\right\}\right]-\frac{1}{12}\left[\left[K^{(2)},X^{H}\right],X^{H}\right]$$

$$H_{0}=R^{U}\left(\mathbf{k}=0\right)=\begin{bmatrix} E^{a}\mathbf{I}_{3\times3} & 0_{3\times3} \\ 0_{3\times3} & E^{o}\mathbf{I}_{3\times3} \end{bmatrix} \tag{15}$$

$$Y(\mathbf{k})=\begin{bmatrix} R_{aa}^{U}(\mathbf{k}) & 0_{3\times3} \\ 0_{3\times3} & R_{oo}^{U}(\mathbf{k}) \end{bmatrix}-R^{U}\left(\mathbf{k}=0\right), \ X(\mathbf{k})=\begin{bmatrix} 0_{3\times3} & R_{ao}^{U}(\mathbf{k}) \\ R_{oa}^{U}(\mathbf{k}) & 0_{3\times3} \end{bmatrix}$$

Chapter 5: Fabrication and Measurement Methods

1- Introduction

This chapter is designated for explaining the experiment procedures, fabrication process and measurement method. Three different approaches used to prepare the GaN NWs were briefly explained; however, the final measurements were done on the last approach of preparing the GaN NWs. Then the procedure for collecting the data, characterization of the mechanical properties of the GaN NWs and characterizing the friction coefficient are meticulously explained.

2- Fabrication methods

Three different approaches were used to prepare the GaN NWs. The first approach was a top-down approach using Au-nanoparticles, gold nanoparticles, mask followed by etching processes, a combination of dry and wet etches. The second approach was a bottom-up selective-area epitaxial growth using metal organic chemical vapor deposition (MOCVD) followed by etching processes, a combination of dry and wet etches. The third approach was a top-down approach using nickel (Ni) mask patterned by Interferometer Laser (IL) method followed by etching processes, a combination of dry and wet etches. For all the bottom-up and top-down fabricated the GaN NWs were c-plane $\{0001\}$ and vertical non-polar $\{1\bar{1}00\}$ m-plane sidewalls.

2-1- Top-down approach using nanoparticles mask

The fabrication flowchart for the top-down GaN NWs using nanoparticle mask is presented in figure 6-1-a. First, a planar c-plane n-GaN (Si doped, ~2 μm thickness) were epitaxially grown on c-plane sapphire. Second, gold (Au) nanoparticles with ~100 nm diameter were spin coated on the c-plane planar GaN template. It should be emphasized that the speed of the spin coat can be adjusted to control the density of the GaN NWs at the end of the process. Then an Inductively Coupled Plasma (ICP) was used to etch the planar GaN template (DC voltage 145 V and Plasma RF 500 W) for 10-15 minutes. The etchant was chlorine, Cl_2, accompanied by Argon, Ar, as noble gas to accelerate the etch rate and provide an isotropic etching process. The chlorine flow was set on 20 sccm, and the argon flow was set on 5 sccm. More details are provided in [77].
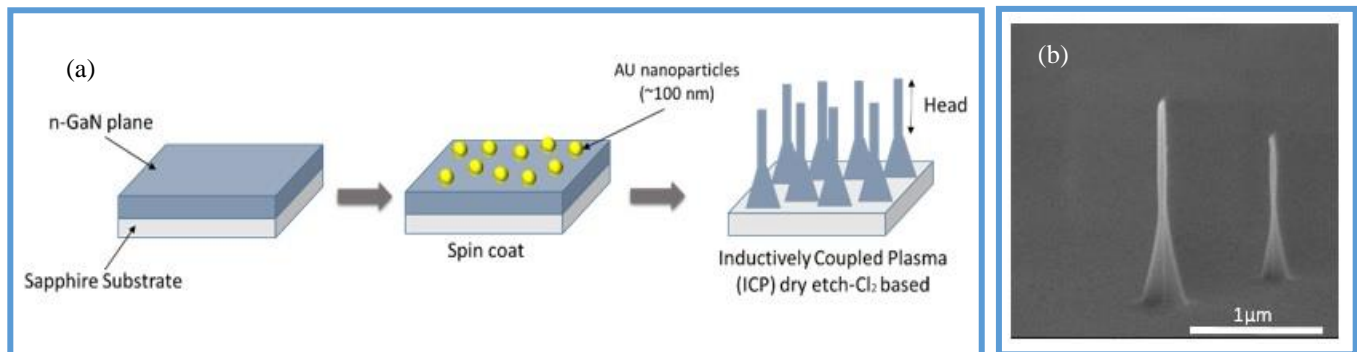

Figure 5-1: fabrication flowchart for top-down GaN NWs using Au nanoparticles mask [77].

Figure 5-1-b indicates an SEM image of the GaN NWs achieved immediately after the ICP dry etch. The GaN NWs fabricated in this way contain a cone-shape base, which tapers to straight walls (~1 μm) near the middle and upper sections of the GaN NWs. That is why the flow of gases becomes more turbulent at vicinity of the substrate in addition to the lower densities of the etchant particles due to higher densities of the etch byproducts at the vicinity of the substrate.

The head diameter of the GaN NWs varies from ~60 nm to 100 nm depending upon the variation in Au nanoparticle diameter used for the dry etch and the degree of dry etch damage from the process. The diameter of the base cone is typically in the range of ~200-400 nm. The GaN NWs obtained using this approach contain damage on sidewalls due to the dry etch process. The results of this approach were not favorable for measuring the mechanical properties of GaN NWs due to variation of the GaN NWs diameters and the nonuniformity of the GaN NWs diameter along their length.

2-2- Bottom-up approach

The procedure for fabricating the bottom-up GaN NWs is the same selective-area epitaxy procedure reported in [78-79]. The process flowchart is illustrated schematically in figure 5-2-a.
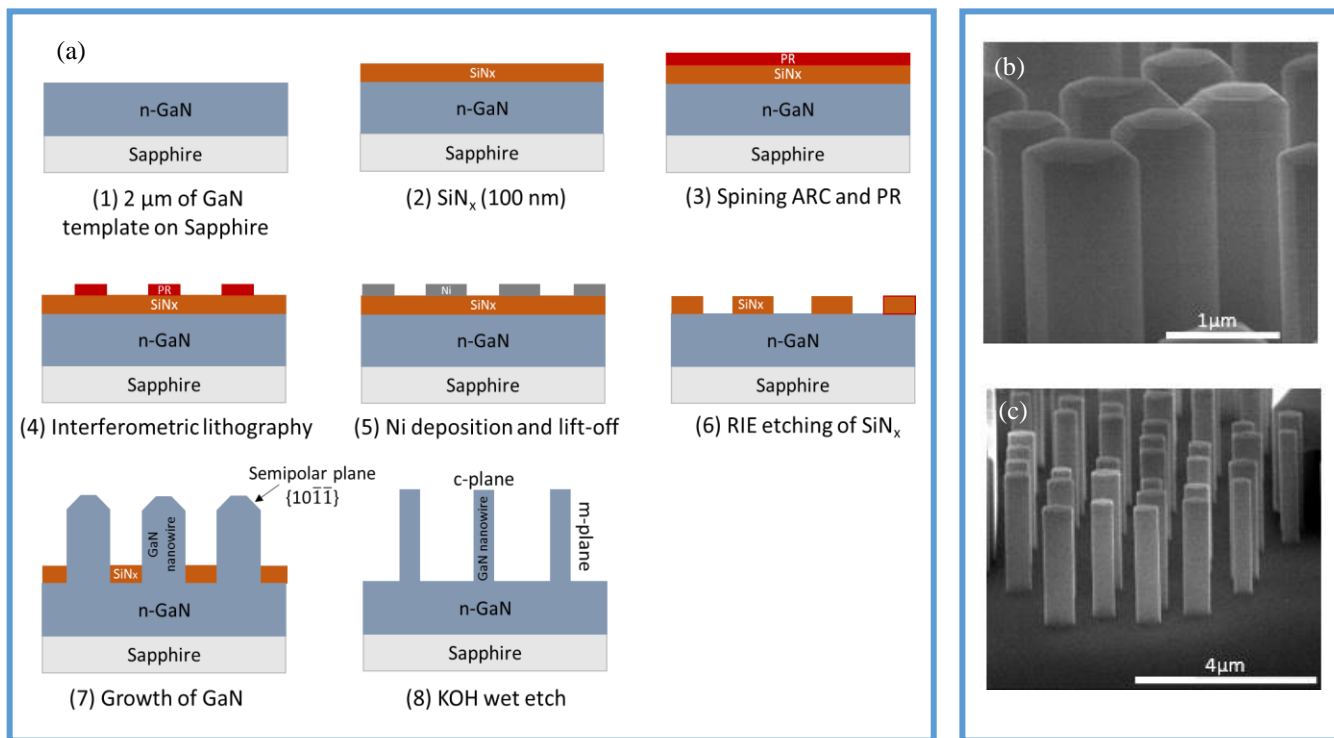

Figure 5-2: fabrication flowchart for bottom-up GaN NWs [77].

48

The sample structure consisted of an ~800 nm thick SiN_x growth-mask layer and a planar MOCVD GaN thin film. The SiN_x mask that was deposited by plasma enhanced chemical vapor deposition had a ~800 nm thickness. The planar GaN that was grown on a 6*H*-SiC substrate had a ~600 nm thickness. The thickness of the SiN_x film was measured using spectrometer. Using IL, the resist was patterned to form hexagonal array of circular openings. After pattering the photoresist, a ~100 nm thick Ni layer was e-beam deposited before removing the photoresist using a spray lift-off process. The pattern was transferred from the Ni film into the silicon nitride layer using Reactive Ion Etching (RIE). Following patterning and just prior to growth, the samples were cleaned in piranha solution for ~5 min followed by rinsing in the distilled water. Lastly, the sample was placed in the MOCVD chamber to grow the GaN NWs.

Semi-polar planes $\{10\overline{1}1\}$ were observed as extra sidewalls on the top of the GaN NWs as seen in figure 5-2-b. To achieve a GaN NW with perfectly straight sidewalls suitable for AFM measurement, the semi-polar planes should be eliminated. Therefore, GaN NWs were immersed in AZ-400K (1:4) at 150°F for 60 minutes. The KOH-based solution is known to be an effective chemical to selectively etch GaN planes, such that the semi-polar planes are removed with a fast etch rate while the c-plane remains unaffected by the solution [80-81] resulting in GaN NWs with smooth sidewalls, figure 5-2-c.

After too many try and errors, this method again could not lead into the favorable GaN NWs for mechanical properties measurement. That is why the minimum diameter of the GaN NWs at the end of wet etch process was 250 nm - 300 nm resulting in small aspect ratios, usually around ~6, while I was interested in measuring the mechanical properties of high aspect ratio GaN NWs with diameters less than 100 nm. The GaN NWs grown using

this method are limited to relatively large diameters since growing high-aspect-ratio nanowire with small diameter (<100 nm) is a challenging due to lateral overgrowth in MOCVD chamber.

2-3- top-down approach using IL patterning

The fabrication flowchart for the top-down GaN NWs is presented in figure 5-3. First, a planar c-plane n-GaN (Si doped, ~2 μm thickness) were epitaxially grown on c-plane sapphire. Second, after spin coating the photoresist on the planar GaN NWs, the IL method was used to fabricate 2D circular patterns with specific pitch sizes and diameters. Third, a thin layer of nickel (Ni) was sputtered using evaporator followed by lift-off process to remove the extra photoresist and the metal. The last step, which was a combination of dry and wet etches, was done the same as explain in section 2-1 of this chapter. During this process the aspect ratio of the GaN NWs is controlled by adjustment of etching time, wet etch solution concentration, solution temperature, and pitch size of the lithography process.

The main difference between this approach and the first approach, section 2-1, is that here the diameter of the metal nanoparticles and the pitch size are precisely controlled and all the metallic nanoparticles have the same diameter. This uniformity results in GaN NWs with extremely uniform distributions over the sample with controlled diameters and aspect ratios appropriate for mechanical properties measurement.
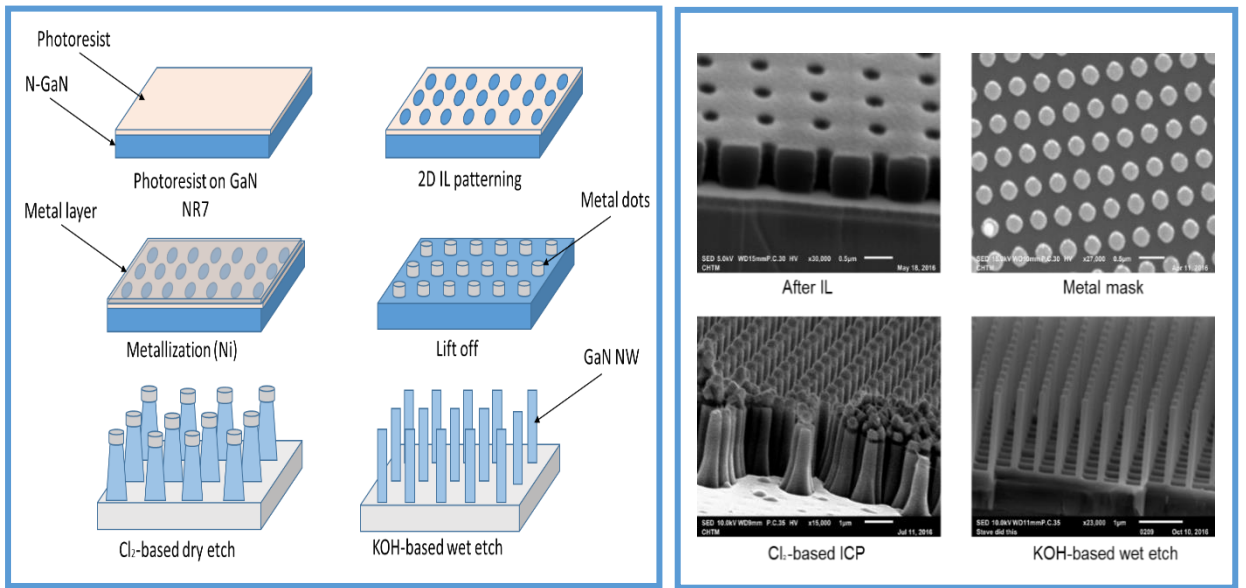
Figure 5-3: fabricated GaN NWs using top-down approach and interferometer laser methods.
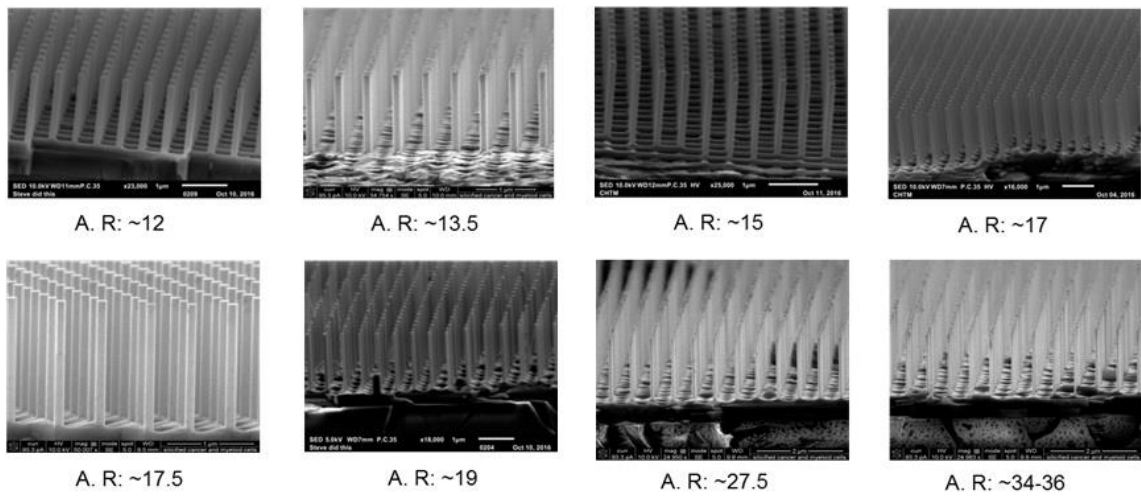

Figure 5-4: final GaN NWs provided for mechanical properties measurement.

Figure 5-4 shows the SEM images of the GaN NWs fabricated using this method for providing high uniform GaN NWs with different aspect ratios from ~12 to ~36.
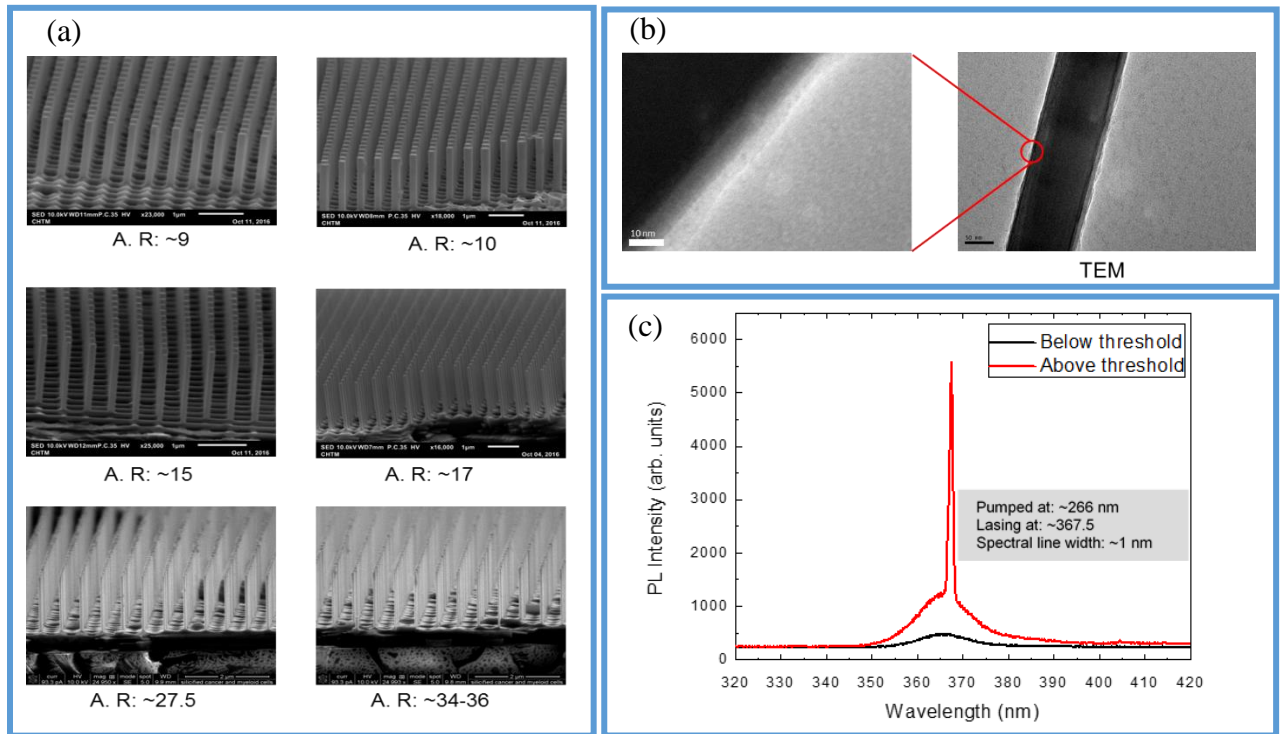
Figure 5-5: (a) NWs fabricated in top-down approach with different aspect ratio. (b) TEM image of fabricated NWs. (c) Laser emission spectrum of NWs pumped at 266 nm.

Sidewall quality of the fabricated GaN NWs were inspected by using TEM, and optical pumping of the GaN NWs. Figure 5-5-b illustrates TEM image of the top-down GaN NWs at the end of fabrication process and figure 5-5-c is the laser emission spectrum of the same GaN NWs. As it can be seen, both TEM and laser emission spectrum results confirm that the quality of the GaN NWs achieved via this process is satisfactory for mechanical properties measurement.

3- Measurement method

The elastic measurements were performed by an AFM (MFP-3D-BIO) instrument. The Silicon-based tips used in this experiment were prepared from Nanoscience Company.

The tips models were Conical Force Modulation (CFM R$^+$). These tips have a conical tip with total cone angle of 30 degrees. The AFM tips have normal spring constant between 3 to 5 nN/nm with rectangular cantilever. Prior to the measurement, I took a very high resolution topography image over an area including couple of GaN NWs, usually including nine GaN NWs per each scanning area. Using the topography image, I set the AFM tip on top of a GaN NW and very close to the GaN NW edge. The AFM tip was set in such a way the axial axis of the AFM sharp tip was parallel to the axial axis of the GaN NW and their common perpendicular, a fictitious line perpendicular to the both GaN NW's axial axis and AFM tip axial axis, was perpendicular to the AFM cantilever as well, see figure 5-6. In this way, I managed to minimize the errors due to the misalignments. It should be emphasized that this misalignment only affects the lateral deflection and torsion of the AFM cantilever that I considered them into the model as it will be explained section 3-2 of this chapter. Furthermore, the results are based on the normal deflection of the AFM cantilever, not lateral or torsional deflections. Thus, the mechanical properties measured in this method are immune from any possible misalignments.
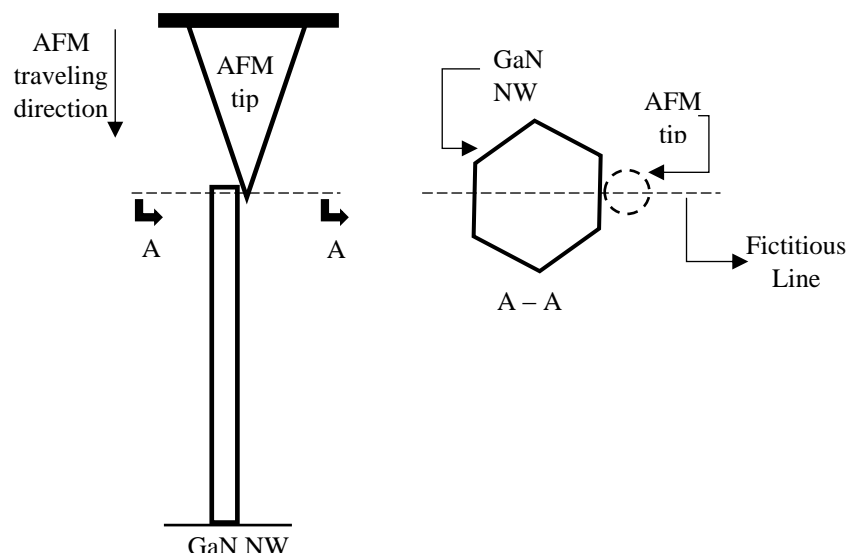

Figure 5-6: initial position of the AFM tip with the GaN NW.

Lastly, I determined a very small vertical displacement for the AFM tip while it is recording the normal and lateral displacements of the AFM tip. Before the tip touches the GaN NW, the normal and lateral displacements of the AFM tip versus the vertical distance was constant, no increases in the normal and lateral displacements. When the tip meets the GaN NW, loading cycle, the normal and lateral displacements of the AFM tip increase almost linearly as the GaN NW is elastically bent from its equilibrium position. During unloading cycle, the normal and lateral displacements drop suddenly at where the AFM tip loses its contact with the GaN NW and reaches its ordinary condition, equilibrium condition. Figure 5-7 shows the acquired plot for loading and unloading cycles.

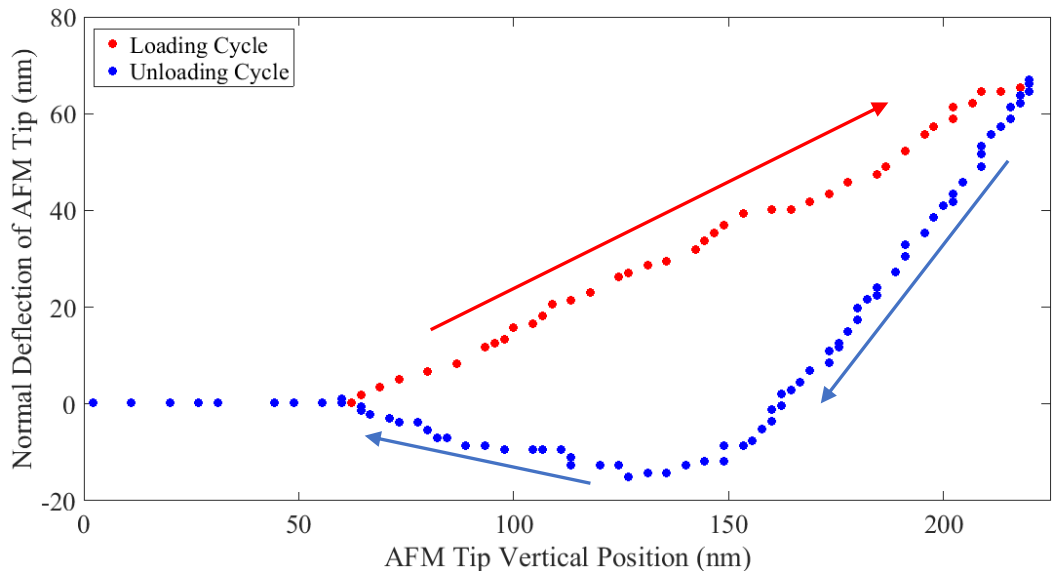Figure 5-7: collected data using AFM during loading cycle (red dots) and unloading cycle (blue dots).

I noticed that loading and unloading plots were started and ended at the same point. This behavior explains that the GaN NWs are acting completely linear elastic for small deformations [27, 82]. Considering the size of the GaN NW, the thermal vibration of the GaN NW at room temperature can be ignored [83].

4- Friction Coefficient characterization

The friction between GaN NW and the AFM tip is one of the most important parameter during the experiment that needs to be taken into consideration and characterized. The friction can be defined as a product of a friction coefficient and the normal force applying onto the conical shape of the AFM tip, f_n, as can be seen in figure 5-8. The friction coefficient can be defined as the ratio of the lateral force to the normal force applying onto the AFM tip as well. The friction coefficient is a function of the quality of the AFM tip and the GaN NWs surfaces, the angle of the AFM tip and electrostatic forces between the AFM tip and the GaN NWs.
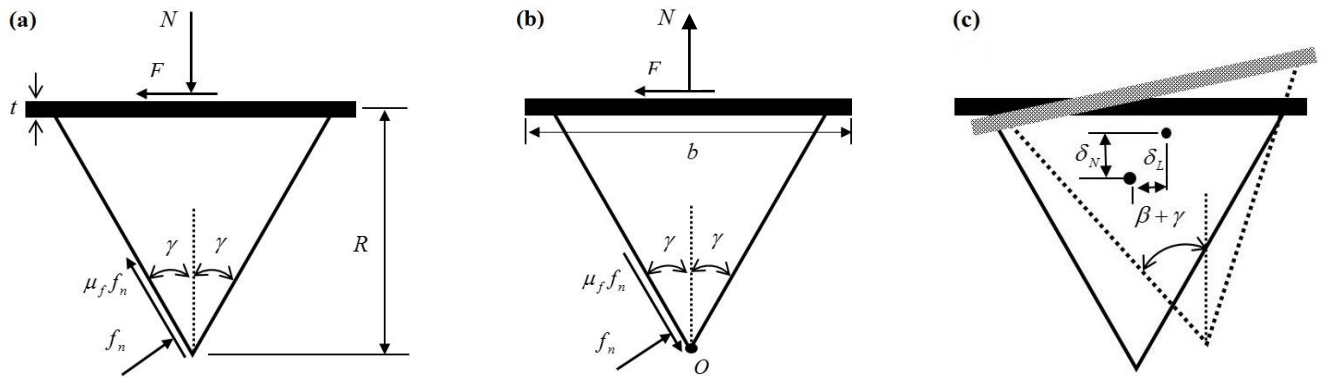
Figure 5-8: applied forces on the AFM's tip during loading, (a), and unloading, (b), and the total deflection of the AFM's tip (c).

When the AFM tip is very close to a GaN NW, the electrostatic force has the highest effects, applying either attractive force or repulsive force. However, the effects of electrostatic forces disappear once the AFM tip is far away from the GaN NW or in contact with the GaN NW. Therefore, the effects of the electrostatic force are negligible. Regarding to this fact, the quality of the AFM tip surface and GaN NW edge is the only source of

friction. In order to characterize the effects of the friction, I monitored the normal deflection of the AFM tip in both loading and unloading cycles. Collecting the normal force in both loading and unloading results in two sets of data for measuring the values of the friction and the mechanical properties of the GaN NW. In order to consider the effects of friction in formula, I wrote the equilibrium equations for the AFM tip during loading and unloading cycles. It should be emphasized, during the loading and unloading, the both normal and lateral forces exerting on the GaN NWs have the same directions while only the direction of the friction between the AFM's tip and the GaN NWs changes. According to figure 5-8, writing the equilibrium equations in $x-$ and $y-$ direction for loading cycle give

$$\sum f_x = 0 \implies -F + f_n \cos(\gamma) - f_n \mu_f \sin(\gamma) = 0 \tag{1}$$

$$\sum f_y = 0 \implies -N + f_n \mu_f \cos(\gamma) + f_n \sin(\gamma) = 0 \tag{2}$$

Dividing the Eq. (1) by Eq. (2) and simplifying the result, it gives

$$\frac{F}{N} = \frac{1 - \mu_f \tan(\gamma)}{\tan(\gamma) + \mu_f} = \frac{1}{\tan(\alpha + \gamma)} \tag{3}$$

In the above equation, μ_f is the friction coefficient between the AFM's tip and the GaN NW which is defined as $\mu_f = \tan(\alpha)$. Utilizing the same procedure for unloading cycle, it leads to

$$\sum f_x = 0 \implies -F + f_n \cos(\gamma) + f_n \mu_f \sin(\gamma) = 0 \tag{4}$$

$$\sum f_y = 0 \implies -N - f_n \mu_f \cos(\gamma) + f_n \sin(\gamma) = 0 \tag{5}$$

Finally,

$$\frac{F}{N} = \frac{1 + \mu_f \tan(\gamma)}{\tan(\gamma) - \mu_f} = \frac{1}{\tan(\gamma - \alpha)} \tag{6}$$

Substituting the above relationships into the solution of the governing equation, one has a system of two nonlinear equations that can be solved for α and k, for the case of the MCST, using the Newton-Raphson method.

5- Normal, Lateral and torsional deflections of AFM tip

The vertical distance traveled by the AFM's tip can be related to the maximum deflection of the GaN NW and the deflection of the AFM tip as follows

$$w_0 + \delta_{AFM} = \Delta h \tan(\gamma + \beta) \tag{7}$$

where δ_{AFM} is the total deflection of the AFM's tip which is a summation of the normal, δ_N, lateral, δ_L, and torsional, δ_T, deflections of the AFM's tip as $\delta_{AFM} = \delta_N \tan(\gamma + \beta) + \delta_L + \delta_T$. Also Δh is the distance traveled by the AFM's tip after touching the GaN NWs, where the normal force increases as the AFM's tip moves downward. In Eq. (7), β is the rotation angle of the AFM's tip, in which $\delta_T = R\beta$. The normal deflection is measured by the AFM gives the normal and lateral forces, Eq. (3) and Eq. (6). In order to find the lateral stiffness, k_L, and torsional stiffness, k_T, I used the normal stiffness of the AFM cantilever estimated by AFM and the geometrical dimensions of the AFM cantilever. The lateral stiffness and the torsional stiffness for a rectangular cross-section are [84]

$$k_L = \frac{F}{\delta_L} = \frac{E_{AFM} b^3 t}{4 L_{AFM}^3} = \left(\frac{b}{t}\right)^2 k_N \tag{8}$$

$$k_T = \frac{T}{\delta_T} = \frac{E_{AFM}\,t^3 b}{6RL_{AFM}\left(1+v_{AFM}\right)} = \left(\frac{2L_{AFM}^2}{3R\left(1+v_{AFM}\right)}\right)k_N \tag{9}$$

where t, b and L_{AFM} are the AFM's cantilever thickness, width and length, respectively. In addition, the v_{AFM} is the AFM's Poisson ratio, the AFM's cantilever was silicon. In Eq. (9), T is the total torsion applied on the AFM's tip determined using torsion equilibrium condition at the point O in figure 5-8. Since the normal and the friction forces intersect at this point, they do not contribute anything to calculation of the torsion. Moreover, since I placed the AFM's tip very close to the GaN NWs edge, the torsion due to f_n is negligible comparing to the torsion due to the lateral force, F. That is why the length of the AFM tips, R, is several micrometers, for these tips it is $12-15\,\mu m$, while the distance between the point O and f_n is in order of nanometer. Therefore, the total exerted torsion on the AFM's tip with a good approximation is $T = RF$, which is equivalent to

$$T = \frac{RN}{\tan(\gamma + \beta \pm \alpha)}.$$

Chapter 6: Results and Discussions

1- Introduction

The experimental results are presented in this chapter. First, I used the MCST formula to evaluate the mechanical properties of the GaN NWs, the Young's modulus and the length scale. Second, I used the MSGT formula to evaluate the mechanical properties of the GaN NWs as well. Then I compare the results of these theories with the results obtained using the CCT. Lastly, I explain the inconsistency between the previous literatures and compare their results with this result.
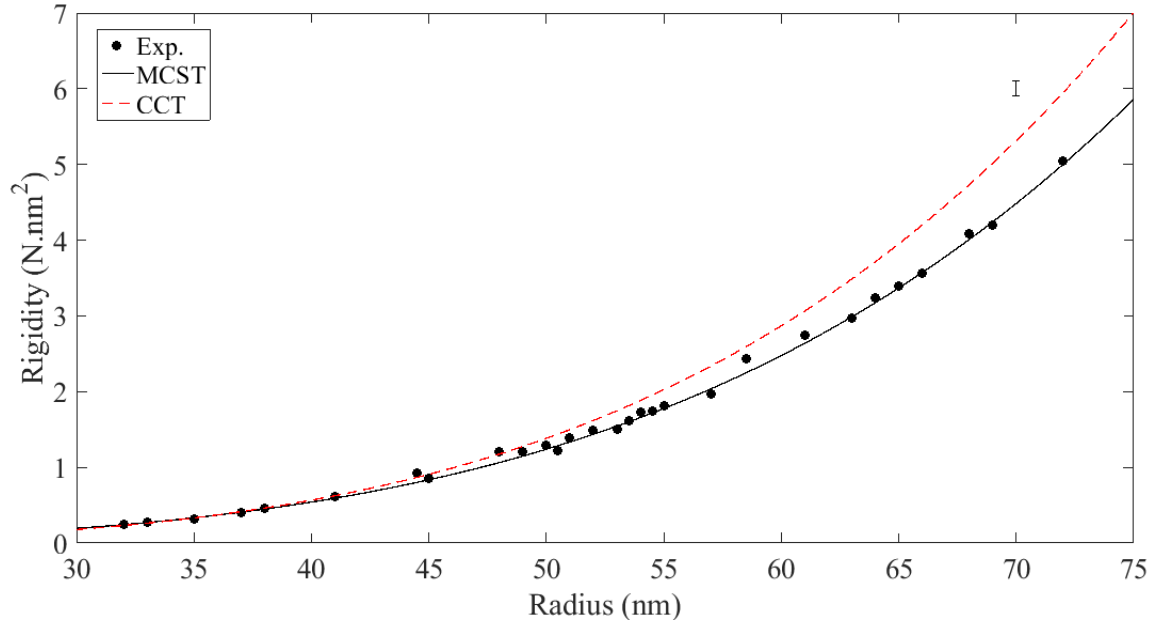
2- Mechanical properties of GaN NWs based on the MCST

By substituting Eq. (3) from chapter 5 into Eq. (36) from chapter 2 for loading and Eq. (6) from chapter 5 into Eq. (36) from chapter 2 for unloading, we have two nonlinear equations that they can be solved using the Newton-Raphson method for the unknown parameters, the friction coefficient and the rigidity of the GaN NWs. The rigidity of the GaN NWs is a function of dimensions and the mechanical properties of the GaN NWs. Interpreting the results for rigidity using the MCST, considering the micro-rotations, resulted in very uniform values for the Young's modulus and the length scale of the GaN NWs. In contrast, the CCT predicts very scatter values for the Young's modulus. I found the results are almost insensitive to the small variations of the Poisson ratio, v, so that I considered the Poisson ratio 0.211, as reported by both experimental and theoretical works [36, 39], to relate the Young's modulus to the shear modulus through $\mu = E\big/2(1+v)$.
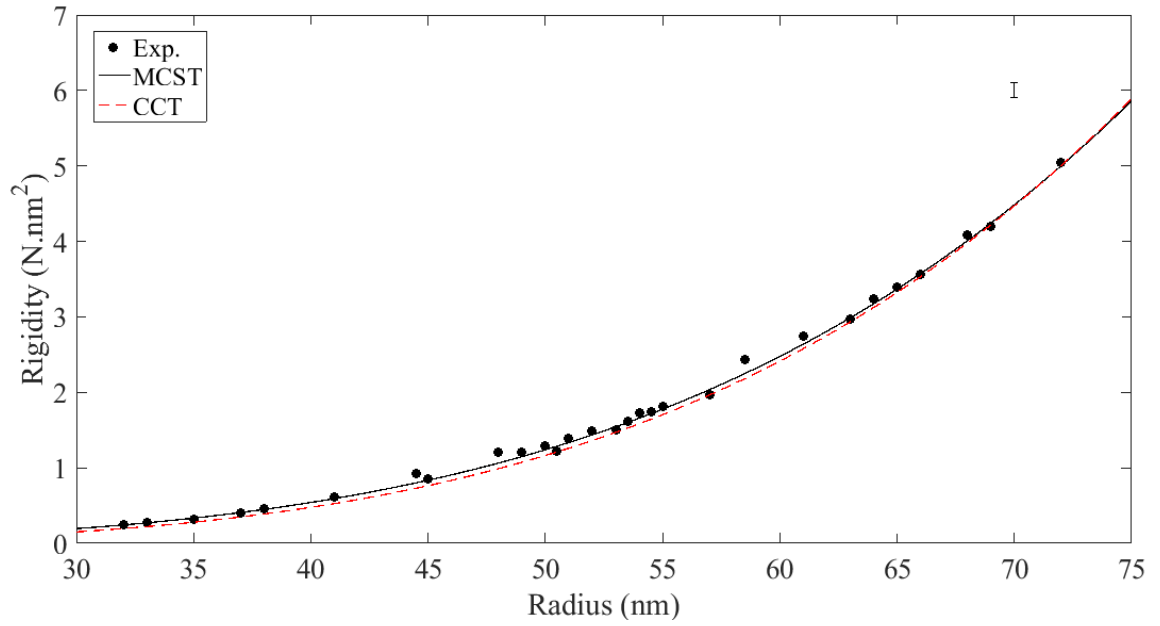
In figure 6-1, I fitted the experimental results for the rigidity, considering $EI + \mu Al^2$ based on the MCST and $E_{CCT}I$ based on the CCT. I added the subscript CCT to the Young's modulus to distinguish between the measured values based on the CCT and the MSCT. The MCST covers all the data points very well for the whole range of radii offering 323 GPa for the Young's modulus and 13 nm for the length scale. In contrast, the CCT results significantly depend on the radii. Figures 6-1 and 6-2 show how the CCT divergences from the experimental data for both small and large radii.

In figure 6-1-a, I fitted the CCT for radii with less than 38 nm, where the Young's modulus was estimated to be 409 GPa, while its value is 344 GPa for the radii larger than 65 nm shown in figure 6-1-b. The large difference in the Young's moduli shows the CCT is unable to capture the size-dependency of the GaN NWs. Indeed, the CCT results are highly dependent on the radii since the CCT does not take into account the micro-rotations.

On the other hand, because the MCST considers the micro-rotations with defining the length scale into the governing equation, it predicts the rigidity of the GaN NWs very precisely for all range of radii. Equivalently, the CCT is applicable only for short ranges of aspect ratio and it always overestimates the Young's modulus due to ignoring the micro-rotation effects which is a crucial fact in determining size-dependency of the mechanical properties of the GaN NWs, and all nanostructures.

(a)

(b)

61
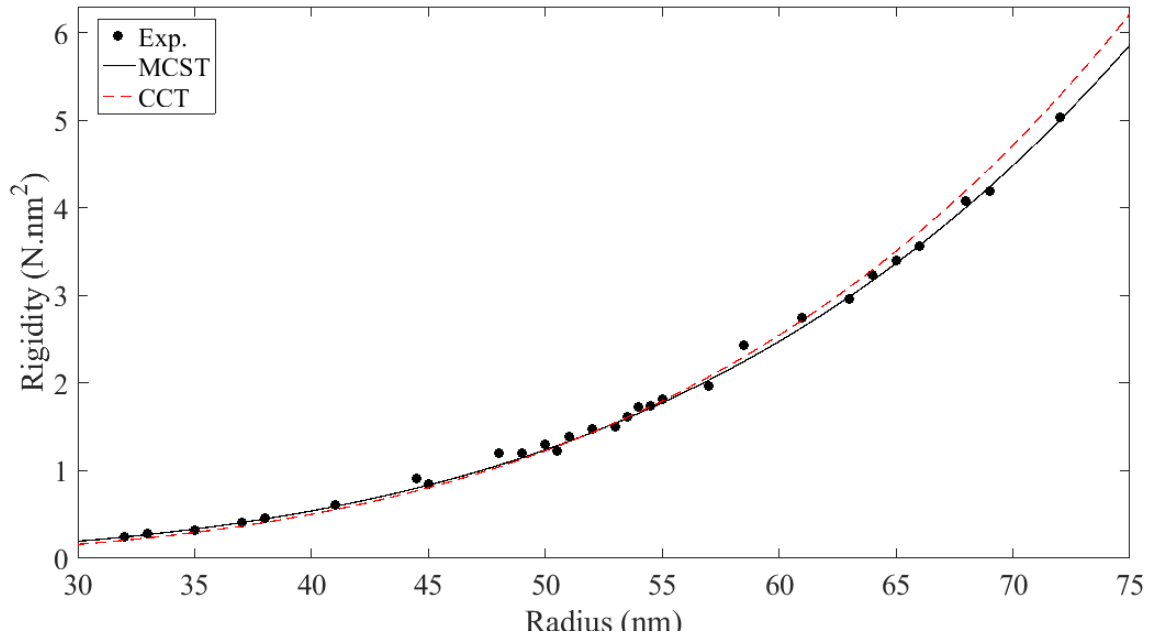
(c)

Figure 6-1: fitted results of CCT for (a) radius < 38 nm, (b) radius > 65 nm, and (c) 50 nm < radius < 60 nm.

MCST covers all data points very well, error is 0.2%, while CCT cannot cover all data points.

Figure 6-2: Zoomed in on different radii. The experimental data were fitted using the CCT for radii within 50 nm to 65 nm with considering the Young's modulus of 363 Gpa.
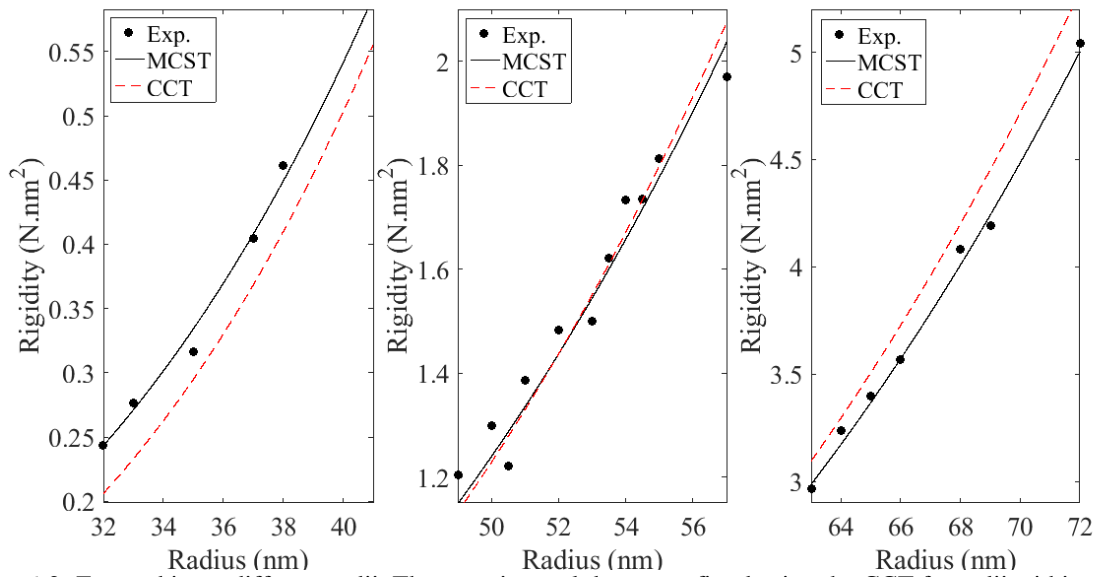
62

3- Mechanical properties of GaN NWs based on the MSGT

By substituting Eq. (3) from chapter 5 into Eq. (44) from chapter 3 for loading and Eq. (6) from chapter 5 into Eq. (44) from chapter 3 for unloading, we again have two nonlinear equations that they can be solved using the Newton-Raphson method for the unknown parameters. Interpreting the experimental data using the MSGT, considering the higher-order strain gradients, resulted in very uniform values for the Young's modulus and the length scale of the GaN NWs. In contrast, the CCT predicts very scatter values for the Young's modulus. Here, the Poisson's ratio assumed to be 0.211 as explained the in section 2.

I firstly used the CCT to predicted the Young's modulus based on CCT and the friction between the surfaces. Since the friction only depends on the conditions of surfaces, I implemented the measured values for friction into the MSGT. Noted the results for the Young's modulus based on the CCT are the same as section 2, thus I avoided repeating CCT's results here again. For simplicity, I consider all the length scales equal, $l_i = l_s$ [65]. Then, I utilized the measured J to predict the length scale as follows

$$l_s = \sqrt{\frac{225(1+v)IJ}{315I - 359AJ}} \tag{8}$$

Using J and P, the S and K can be easily determined, which they can be used to estimate the Young's modulus of the GaN NWs.

The results for S and K/l_s^2 are plotted in figures 6-3 and 6-4, respectively. The best fit for the K/l_s^2 gives 132 Gpa as the shear modulus. Considering the Poisson ratio 0.211, the best fit for S results in 319 Gpa for the Young's modulus and 8 nm for the length scale.
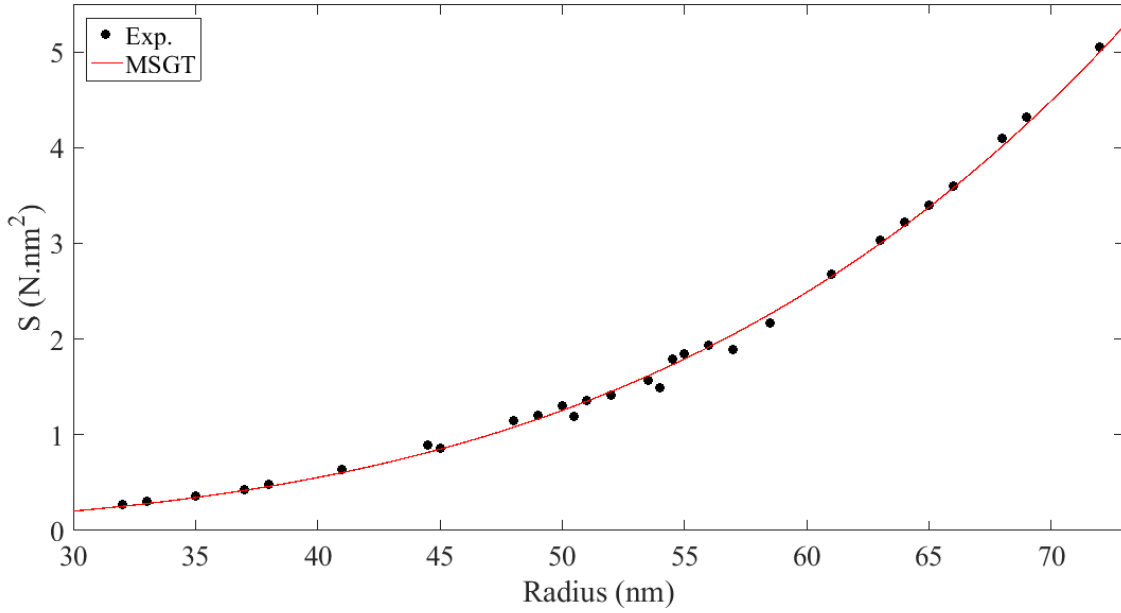
Figure 6-3: measured S experimentally for each GaN NWs (circles) and MSGT fitting (solid line).
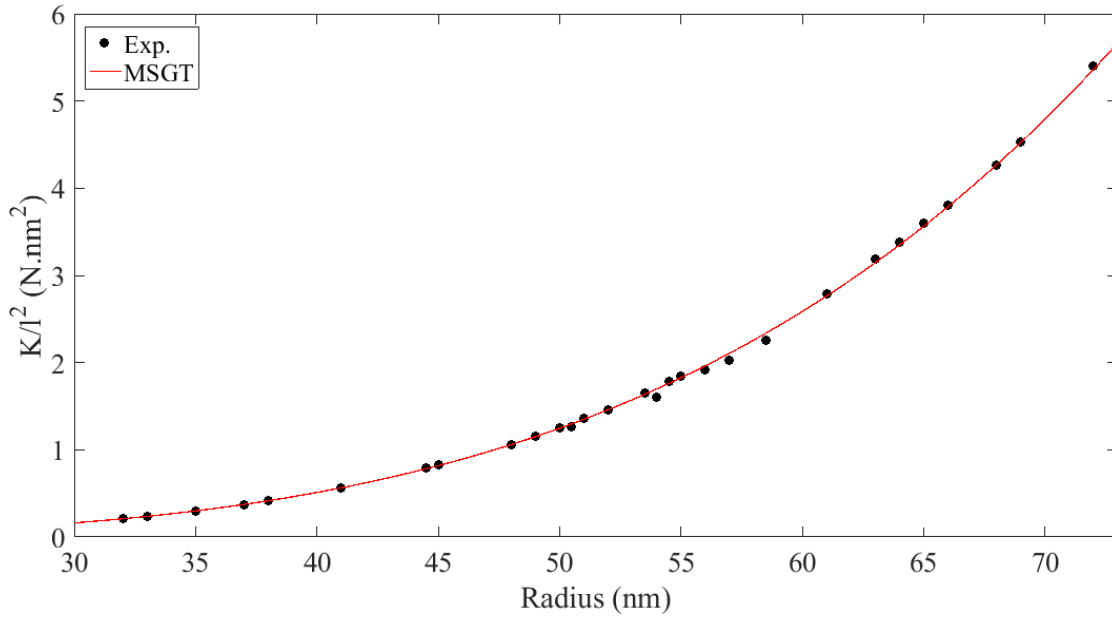

Figure 6-4: K/l_s^2 measured experimentally based on MSGT.

In a professional point of view, no one can compare the MSGT with the CCT or even the MCST together because the natures of their governing equations are different.

The governing equation based on MSGT is a 6th order differential equations while the governing equation based on the CCT, even the MCST, is a 4th order differential equation. Regarding to this difference, the concepts of rigidity in these two theories are different. However, it is possible to define an equivalent Young's modulus according to the MCST and the MSGT usable to comparison these three theories with each other. In the next section, these three theories are compared to each other using the equivalent Young's modulus definition.

4- Comparing the results with previous studies

Figure 6-6 shows the equivalent Young's modulus of the GaN NWs defined based on the CCT, the MSGT and the MCST. I provided figure 6-6 to illustrate the effects of micro-rotations and higher strain gradients on the mechanical behaviors of GaN NWs and the size-dependency of the mechanical properties of GaN NWs. That is why some studies show that the Young's modulus of the GaN NWs decreases as the GaN NWs radius decreases [25, 85], while other studies show that the Young's modulus increases as the radius decreases, for example [23, 26-27]. To understand this discrepancy, first I must define the equivalent Young's modulus. To do so, I found the relationship of the maximum deflection of a cantilever GaN NWs, fixed-free boundary condition as shows in figure 6-5, based on the MCST, the MSGT and the CCT, under a concentrated force, $G_i\,(i=CCT,\,MSCT,\,MSGT)$. Then utilizing these relationships, I figured out the equivalent Young's modulus, $E_{Eq-i}\,(i=CCT,\,MSCT,\,MSGT)$.

$$w_0 = G_i F$$
$$i = CCT, MCST, MSGT$$
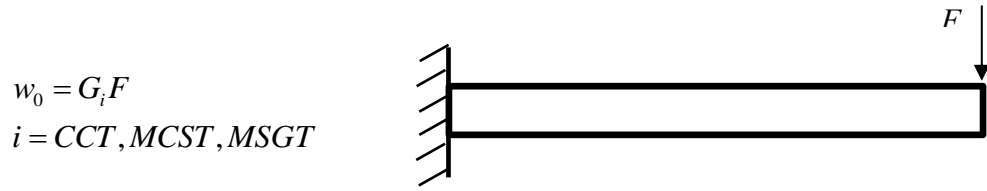
Figure 6-5: a cantilever GaN NW under a concentrated force at its free end.

After finding E_{Eq-i} based on each theory, I plugged the Young's modulus and the length scale predicted in sections 2 and 3 of this chapter into $E_{Eq-MCST}$ and $E_{Eq-MSGT}$ relationships, then I plotted them vs. radius in figure 6-6.

In figure 6-6 shows the normalized E_{Bulk}, E_{CCT}, E_{MCST} and E_{MSGT} with respect to the Young's modulus of bulk GaN [86], the values of the Young's modulus for each individual GaN NWs using the CCT, the MCST and the MSGT, respectively.
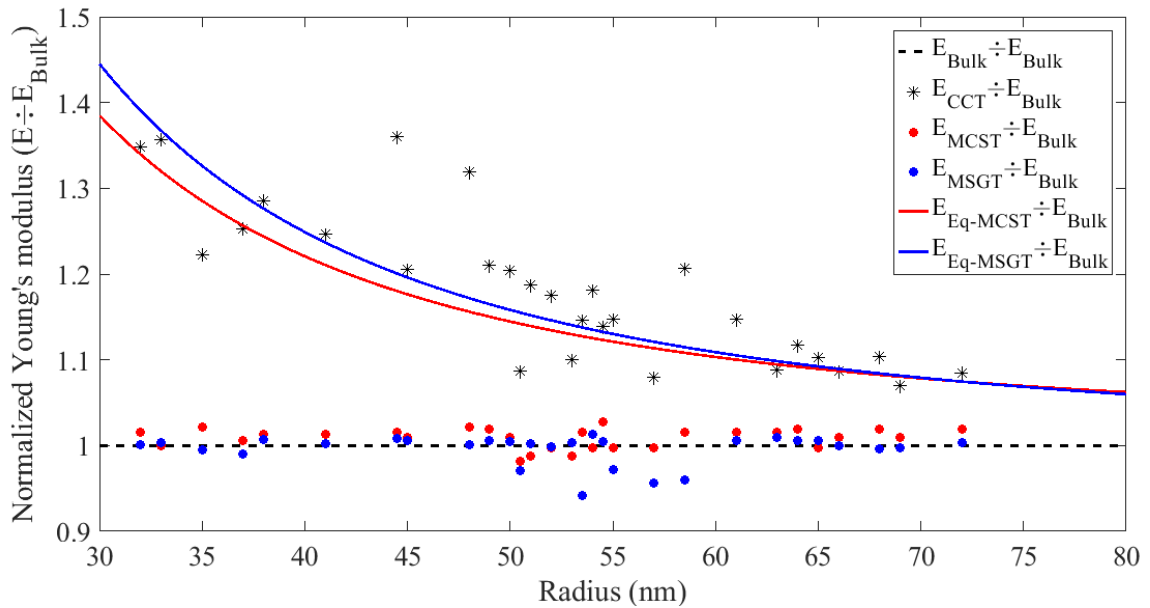
Figure 6-6: Experimentally measured Young's modulus as a function of radius of GaN NWs and then normalized respect to the Young's modulus of the bulk GaN. The dots and stars are the experimental results for each GaN NW. The slid lines are the equivalent Young's modulus, and the dashed line is the Young's modulus of bulk GaN.

According to figure 6-6, the Young's moduli predicted by all theories converge to each other as the radius increases. According to the Cosserats theory [45], as the dimensions of the nanostructures increases toward the bulk values, the effects of strain gradients on the rigidity decreases. Indeed, the both theories are the same for bulk dimensions, and the size-dependency of mechanical properties of materials vanishes at bulk dimensions. However, reducing the radius of the GaN NWs to less than ~50 nm significantly increases the size-dependency of the GaN NWs. It should be emphasized that the results of the MCST and the MSGT are slightly different at small radii. That is why the MCST only considers only the 2st order strain gradient in its governing equation while the MSGT considers up to 3rd order strain gradients in its governing equations.

Table 6-1 provides a comprehensive comparison of the Young's modulus of GaN NWs estimated with different experimental and theoretical techniques. As it can be seen, the MCST and the MSGT suggest only a single value for the Young's modulus of GaN NWs while the CCT, which used in all earlier literatures and even this results, suggest a wide domain the Young's modulus.

Table 6-1: experimental and theoretical on the Young's modulus of GaN.

	Method	Young's modulus (GPa)		Length Scale (nm)	Ref.
		Max.	Min.		
Experimentally	Present Work (MSGT)	319		8	-
	Present Work (MCST)	323		13	-
	Present Work (CCT)	409	344	-	-
	Three-point bending	400	194	-	[30]
	Electromechanical resonator	305	227	-	[27]
	Nanoindentation	292	298	-	[31]

	Laser Doppler vibrometry	321	201	-	[32]
	Uniaxial tensile test	250	210	-	[23]
	Uniaxial compression test	484	223	-	[24]
	in situ TEM	319	280	-	[26]
		404	258	-	[33]
Theoretically	First principle	444		-	[37]
	Electron backscatter diffraction	479		-	[38]
	Molecular dynamic simulation	290	166	-	[21]

It is worthy to be mentioned, the Young's modulus of the present GaN NWs based on the CCT are a little larger than the reported in some literatures, see table 6-1, which can be attributed to the nature of the experiment. I implemented measurements on the GaN NWs directly after their fabrication, without any manipulation of the GaN NWs which is never the case for any other methods. For example, the GaN NWs are cut and transferred on a trench, for three-point bending [30], or a MEMS device, for tensile test [23], and then welded on the new substrate. These processes cause partial fracture of GaN NWs and contaminations, which drastically affect the mechanical properties of GaN NWs [43].

Furthermore, because of the strong bonding between the GaN NWs and the substrate, GaN-GaN, in the present experiment, there were neither any elastic deformations nor violation of the boundary conditions at the fixed end of the GaN NWs, which their existences cause misleading in predicting the mechanical properties of nanostructures [40-42].

Conclusion

In this thesis, the classical, the Young's modulus and shear modulus, and non-classical, the length scale parameter, mechanical properties of GaN NWs were measured using the CCT, the MCST and MSGT. The MCST estimates the Young's modulus, the shear modulus and the length scale to be 323 GPa, 133 GPa and 13 nm, respectively. And the MSGT estimated the Young's modulus, the shear modulus and the length scale to be 319 GPa, 132 GPa and 8 nm, respectively. Comparing the results of the MCST and the MSGT, it cannot be easily concluded that the MCST predicts the GaN NWs stiffer than the MSGT because of slightly higher values of the both classical and non-classical properties of the GaN NWs. For a precise comparison, the equivalent Young's modulus should be considered. That is why the theories governing equations are completely different which results in different concepts of rigidity and stiffness. Furthermore, the CCT was used to estimate the Young's modulus of the GaN NWs. The CCT estimates the Young's modulus of the GaN NWs varies from 409 GPa to 344 GPa as the radius increases. Comparing the results of the MSGT, the MCST and the CCT, the inconsistencies appearing in earlier publication on mechanical properties of GaN NWs were clearly explained.

Future works

The future works on the GaN-based NWs is going toward smaller and smaller dimensions which requires a comprehensive development of non-classical properties of GaN NWs. Consequently, it is crucial to measure the mechanical properties of GaN NWs in smaller dimensions. In smaller dimensions, the non-classical theories need to be modified to consider the effects of defects, such as vacancies, interstitial impurities, on

covalent bonds in the form of higher strain gradients. Therefore, one of the future work is to develop a modified non-classical theory including the effects of covalent bonding in its governing equation and to validate them using experimental measurements.

Moreover, because the GaN NWs are mainly doped in nano-devices, such as LEDs and piezoelectric devices, it is essential to study the classical and non-classical properties of GaN NWs with different levels of doping. One way is to dope the GaN template before starting the fabrication process. It should be emphasized that the level of doping a critical parameter for preparing the GaN NWs and performance of the GaN NWs.

Furthermore, regarding to the piezoelectric applications of the GaN NWs, it is essential to study the dynamical behavior of the GaN NWs especially at high frequencies. That is why the piezoelectric coefficients, which relates the mechanical strains to the electrical current, are the critical parameters for determining the piezoelectric behavior of the GaN NWs. Therefore, they must be estimated under precisely demonstrated mechanical deformations/strains.

References

[1]: Nakamura, Shuji, Stephen Pearton, and Gerhard Fasol. *The blue laser diode: the complete story*. Springer Science & Business Media, 2013.

[2]: Goldberger, Joshua, et al. "Single-crystal gallium nitride nanotubes." *Nature* 422.6932 (2003): 599-602.

[3]: Westover, Tyler, et al. "Photoluminescence, thermal transport, and breakdown in Joule-heated GaN nanowires." *Nano letters* 9.1 (2008): 257-263.

[4]: Hersee, Stephen D., Xinyu Sun, and Xin Wang. "The controlled growth of GaN nanowires." *Nano letters* 6.8 (2006): 1808-1811.

[5]: Shul, RJa, et al. "Comparison of plasma etch techniques for III–V nitrides." *Solid-State Electronics* 42.12 (1998): 2259-2267.

[6]: Beach, R. A., and T. C. McGill. "Piezoelectric fields in nitride devices." *Journal of Vacuum Science & Technology B* 17.4 (1999): 1753-1756.

[7]: Minary-Jolandan, Majid, et al. "Individual GaN nanowires exhibit strong piezoelectricity in 3D." *Nano letters* 12.2 (2012): 970-976.

[8]: Weber, J. C., et al. "Gallium nitride nanowire probe for near-field scanning microwave microscopy." *Applied Physics Letters* 104.2 (2014): 023113.

[9]: Bao, Wei, et al. "Carrier Localization Effects in InGaN/GaN Multiple-Quantum-Wells LED Nanowires: Luminescence Quantum Efficiency Improvement and "Negative" Thermal Activation Energy." *Scientific Reports* 6 (2016).

[10]: Duan, Xiangfeng, and Charles M. Lieber. "Laser-assisted catalytic growth of single crystal GaN nanowires." *Journal of the American Chemical Society* 122.1 (2000): 188-189.

[11]: Liu, Baodan, et al. "Wurtzite-type faceted single-crystalline GaN nanotubes." *Applied physics letters* 88.9 (2006): 93120-93120.

[12]: Ishida, Akihiro, et al. "Design and preparation of AlN/GaN quantum wells for quantum cascade laser applications." *Japanese journal of applied physics* 44.8R (2005): 5918.

[13]: Winkler, Holger, et al. "Quantum-Confined Gallium Nitride in MCM-41." *Advanced materials* 11.17 (1999): 1444-1448.

[14]: Dayeh, Shadi A., Anna Fontcuberta i Morral, and Chennupati Jagadish. *Semiconductor Nanowires II: Properties and Applications*. Vol. 94. Academic Press, 2016.

[15]: Rieger, W., et al. "Influence of substrate-induced biaxial compressive stress on the optical properties of thin GaN films." *Applied physics letters* 68.7 (1996): 970-972.

[16]: Kim, Kwiseon, Walter RL Lambrecht, and Benjamin Segall. "Electronic structure of GaN with strain and phonon distortions." *Physical Review B* 50.3 (1994): 1502.

[17]: Signorello, G., et al. "Inducing a direct-to-pseudodirect bandgap transition in wurtzite GaAs nanowires with uniaxial stress." *Nature communications* 5 (2014).

[18]: Wen, Yu-Hua, Zi-Zhong Zhu, and Ru-Zeng Zhu. "Molecular dynamics study of the mechanical behavior of nickel nanowire: Strain rate effects." *Computational Materials Science* 41.4 (2008): 553-560.

[19]: Wang, Zhiguo, et al. "Atomistic simulation of brittle to ductile transition in GaN nanotubes." *Applied physics letters* 89.24 (2006): 243123.

[20]: Le, Minh-Quy. "Atomistic study on the tensile properties of hexagonal AlN, BN, GaN, InN and SiC sheets." *Journal of Computational and Theoretical Nanoscience* 11.6 (2014): 1458-1464.

[21]: Wang, Zhiguo, et al. "Mechanical behavior of gallium nitride nanotubes under combined tension-torsion: An atomistic simulation." *Journal of Applied Physics* 103.1 (2008): 013505.

[22]: Wang, Guofeng, and Xiaodong Li. "Predicting Young's modulus of nanowires from first-principles calculations on their surface and bulk materials." *Journal of Applied Physics* 104.11 (2008): 113517.

[23]: Brown, J. J., et al. "Tensile measurement of single crystal gallium nitride nanowires on MEMS test stages." *Sensors and Actuators A: Physical* 166.2 (2011): 177-186.

[24]: Wang, Zhiguo, et al. "Buckling of GaN nanotubes under uniaxial compression." *Solid State Communications* 146.7 (2008): 293-297.

[25]: Nam, Chang-Yong, et al. "Diameter-dependent electromechanical properties of GaN nanowires." *Nano letters* 6.2 (2006): 153-158.

[26]: Bernal, Rodrigo A., et al. "Effect of growth orientation and diameter on the elasticity of GaN nanowires. A combined in situ TEM and atomistic modeling investigation." *Nano letters* 11.2 (2010): 548-555.

[27]: Huang, Jian Yu, et al. "In situ nanomechanics of GaN nanowires." *Nano letters* 11.4 (2011): 1618-1622.

[28]: Espinosa, Horacio D., Rodrigo A. Bernal, and Tobin Filleter. "In situ TEM electromechanical testing of nanowires and nanotubes." *Small* 8.21 (2012): 3233-3252.

[29]: Ni, Hai, et al. "Elastic modulus of single-crystal GaN nanowires." *Journal of materials research* 21.11 (2006): 2882-2887.

[30]: Chen, Yunxia, et al. "Mechanical elasticity of vapour–liquid–solid grown GaN nanowires." *Nanotechnology* 18.13 (2007): 135708.

[31]: Feng, Gang, et al. "A study of the mechanical properties of nanowires using nanoindentation." *Journal of Applied Physics* 99.7 (2006): 074304.

[32]: Ben Amar, Achraf, et al. "Young's modulus extraction of epitaxial heterostructure AlGaN/GaN for MEMS application." *physica status solidi (a)*211.7 (2014): 1655-1659.

[33]: Dai, Sheng, et al. "Elastic properties of GaN nanowires: Revealing the influence of planar defects on Young's modulus at nanoscale." *Nano letters*15.1 (2014): 8-15.

[34]: Moram, M. A., Z. H. Barber, and C. J. Humphreys. "Accurate experimental determination of the Poisson's ratio of GaN using high-resolution x-ray diffraction." *Journal of applied physics* 102.2 (2007): 023505.

[35]: Polian, A., M. Grimsditch, and I. Grzegory. "Elastic constants of gallium nitride." *Journal of Applied Physics* 79.6 (1996): 3343-3344.

[36]: Davydov, V. Yu, et al. "Raman and photoluminescence studies of biaxial strain in GaN epitaxial layers grown on 6H–SiC." *Journal of applied physics*82.10 (1997): 5097-5102.

[37]: Hoang, M. T., et al. "Size-dependent mechanical properties of axial and radial mixed AlN/GaN nanostructure." *Nanotechnology* 26.11 (2015): 115703.

[38]: Shao, Yongliang, et al. "Large Area Stress Distribution in Crystalline Materials Calculated from Lattice Deformation Identified by Electron Backscatter Diffraction." *Scientific reports* 4 (2014).

[39]: Shimada, Kazuhiro, Takayuki Sota, and Katsuo Suzuki. "First-principles study on electronic and elastic properties of BN, AlN, and GaN." *Journal of Applied Physics* 84.9 (1998): 4951-4958.

[40]: Zhang, Yin, and Ya-Pu Zhao. "Adhesive contact of nanowire in three-point bending test." Journal of Adhesion Science and Technology 25.10 (2011): 1107-1129.

[41]: Gangadean, D., et al. "Winkler boundary conditions for three-point bending tests on 1D nanomaterials." Nanotechnology 21.22 (2010): 225704.

[42]: Keer, L. M., John Dundurs, and K. C. Tsai. "Problems involving a receding contact between a layer and a half space." *Journal of Applied Mechanics*39.4 (1972): 1115-1120.

[43]: Song, Jinhui, et al. "Elastic property of vertically aligned nanowires." Nano Letters 5.10 (2005): 1954-1958.

[44]: Yang, J. F. C., and Roderic S. Lakes. "Experimental study of micropolar and couple stress elasticity in compact bone in bending." *Journal of biomechanics* 15.2 (1982): 91-98.

[45]: Cosserat, E., and F. Cosserat. "Deformable Bodies." *Scientific Library A. Hermann and Sons* (1909).

[46]: Asghari, M., et al. "The modified couple stress functionally graded Timoshenko beam formulation." *Materials & Design* 32.3 (2011): 1435-1443.

[47]: Ma, H. M., X-L. Gao, and J. N. Reddy. "A microstructure-dependent Timoshenko beam model based on a modified couple stress theory." *Journal of the Mechanics and Physics of Solids* 56.12 (2008): 3379-3391.

[48]: Park, S. K., and X. L. Gao. "Bernoulli–Euler beam model based on a modified couple stress theory." *Journal of Micromechanics and Microengineering* 16.11 (2006): 2355.

[49]: Qi, H. J., et al. "Determination of mechanical properties of carbon nanotubes and vertically aligned carbon nanotube forests using nanoindentation."*Journal of the Mechanics and Physics of Solids* 51.11 (2003): 2213-2237.

[50]: Poncharal, Philippe, et al. "Electrostatic deflections and electromechanical resonances of carbon nanotubes." *science* 283.5407 (1999): 1513-1516.

[51]: Gao, Zhiyuan, et al. "Dynamic fatigue studies of ZnO nanowires by in-situ transmission electron microscopy." *physica status solidi (RRL)-Rapid Research Letters* 3.7-8 (2009): 260-262.

[52]: Ryu, Seung Yoon, et al. "Lateral buckling mechanics in silicon nanowires on elastomeric substrates." *Nano letters* 9.9 (2009): 3214-3219.

[53]: Zhu, Yong. "In Situ Nanomechanical Testing of Crystalline Nanowires in Electron Microscopes." *JOM* 68.1 (2016): 84-93.

[54]: Feng, Gang, et al. "A study of the mechanical properties of nanowires using nanoindentation." *Journal of Applied Physics* 99.7 (2006): 074304.

[55]: Truesdell, Clifford, ed. *Linear Theories of Elasticity and Thermoelasticity: Linear and Nonlinear Theories of Rods, Plates, and Shells*. Vol. 2. Springer, 2013.

[56]: Hadjesfandiari, Ali R., and Gary F. Dargush. "Evolution of generalized couple-stress continuum theories: a critical analysis." *arXiv preprint arXiv:1501.03112* (2014).

[57]: Mindlin, R. D., and H. F. Tiersten. "Effects of couple-stresses in linear elasticity." *Archive for Rational Mechanics and analysis* 11.1 (1962): 415-448.

[58]: KOlTER, W. T. "Couple stresses in the theory of elasticity." *Proc. Koninklijke Nederl. Akaad. van Wetensch* 67 (1964).

[59]: Yang, F. A. C. M., et al. "Couple stress based strain gradient theory for elasticity." *International Journal of Solids and Structures* 39.10 (2002): 2731-2743.

[60]: Abadi, M. Mohammad, and A. R. Daneshmehr. "An investigation of modified couple stress theory in buckling analysis of micro composite laminated Euler–Bernoulli and Timoshenko beams." *International Journal of Engineering Science* 75 (2014): 40-53.

[61]: Tsiatas, George C., and Aristophanes J. Yiotis. "A modified couple stress theory for bending, buckling and vibration of skew orthotropic micro-plates." *Proc. 10th HSTAM Int. Congress of Mechanics, Chania*. 2013.

[62]: Mindlin, R. D., and N. N. Eshel. "On first strain-gradient theories in linear elasticity." *International Journal of Solids and Structures* 4.1 (1968): 109-124.

[63]: Fleck, N. A., and J. W. Hutchinson. "A phenomenological theory for strain gradient effects in plasticity." *Journal of the Mechanics and Physics of Solids* 41.12 (1993): 1825-1857.

[64]: Fleck, N. A., and J. W. Hutchinson. "A reformulation of strain gradient plasticity." *Journal of the Mechanics and Physics of Solids* 49.10 (2001): 2245-2271.

[65]: Lam, David CC, et al. "Experiments and theory in strain gradient elasticity." *Journal of the Mechanics and Physics of Solids* 51.8 (2003): 1477-1508.

[66]: Kahrobaiyan, M. H., et al. "A nonlinear strain gradient beam formulation." *International Journal of Engineering Science* 49.11 (2011): 1256-1267.

[67]: Akgöz, B., and Ö. Civalek. "Buckling analysis of cantilever carbon nanotubes using the strain gradient elasticity and modified couple stress theories." *Journal of Computational and Theoretical Nanoscience* 8.9 (2011): 1821-1827.

[68]: Kong, Shengli, et al. "Static and dynamic analysis of micro beams based on strain gradient elasticity theory." *International Journal of Engineering Science* 47.4 (2009): 487-498.

[69]: Akgöz, Bekir, and Ömer Civalek. "Analysis of micro-sized beams for various boundary conditions based on the strain gradient elasticity theory." *Archive of Applied Mechanics* 82.3 (2012): 423-443.

[70]: DiVincenzo, D. P. "Dispersive corrections to continuum elastic theory in cubic crystals." *Physical Review B* 34.8 (1986): 5450.

[71]: Maranganti, R., and P. Sharma. "A novel atomistic approach to determine strain-gradient elasticity constants: Tabulation and comparison for various metals, semiconductors, silica, polymers and the (ir) relevance for nanotechnologies." *Journal of the Mechanics and Physics of Solids* 55.9 (2007): 1823-1852.

[72]: Askes, Harm, and Elias C. Aifantis. "Gradient elasticity in statics and dynamics: an overview of formulations, length scale identification procedures, finite element implementations and new results." *International Journal of Solids and Structures* 48.13 (2011): 1962-1990.

[73]: Giannozzi, Paolo, et al. "Ab initio calculation of phonon dispersions in semiconductors." *Physical Review B* 43.9 (1991): 7231.

[74]: Soler, José M., et al. "The SIESTA method for ab initio order-N materials simulation." *Journal of Physics: Condensed Matter* 14.11 (2002): 2745.

[75]: Maradudin, Alexei A. "Theory of lattice dynamics in the harmonic approximation." (1971).

[76]: Kunc, K., and O. Holm Nielsen. "Lattice dynamics of zincblende structure compounds using deformation-dipole model and rigid ion model." *Computer Physics Communications* 16.2 (1979): 181-197.

[77]: Behzadirad, Mahmoud, et al. "GaN nanowire tips for nanoscale atomic force microscopy." *Nanotechnology* 28.20 (2017): 20LT01.

[78]: Brueck, S. R. J. "Optical and interferometric lithography-nanotechnology enablers." Proceedings of the IEEE 93.10 (2005): 1704-1721.

[79]: Hersee, Stephen D., Xinyu Sun, and Xin Wang. "The controlled growth of GaN nanowires." Nano letters 6.8 (2006): 1808-1811.

[80]: Chen, Weijie, et al. "GaN nanowire fabricated by selective wet-etching of GaN micro truncated-pyramid." Journal of Crystal Growth 426 (2015): 168-172.

[81]: Li, Qiming, et al. "Optical performance of top-down fabricated InGaN/GaN nanorod light emitting diode arrays." Optics express 19.25 (2011): 25528-25534.

[82]: Wang, Zhiguo, et al. "Orientation and temperature dependence of the tensile behavior of GaN nanowires: an atomistic study." *Journal of Materials Science: Materials in Electronics* 19.8-9 (2008): 863-867.

[83]: Treacy, MM JEBBESSEN, T. W. Ebbesen, and J. M. Gibson. "Exceptionally high Young's modulus observed for individual carbon nanotubes." *Nature* 381.6584 (1996): 678.

[84]: Sadd, Martin H. *Elasticity: theory, applications, and numerics*. Academic Press, 2009.

[85]: Gulans, Andris, and Ivars Tale. "Ab initio calculation of wurtzite-type GaN nanowires." physica status solidi (c) 4.3 (2007): 1197-1200.

[86]: Fujikane, Masaki, et al. "Elastic–plastic transition during nanoindentation in bulk GaN crystal." Journal of Alloys and Compounds 450.1 (2008): 405-411.